Production, Purification, and Crystallization Strategies for Recombinant EGFR and HER2 Tyrosine Kinase Domains as a Platform for Structure-Based Drug Discovery

by

Edanur Topalan

A Dissertation Submitted to the
Graduate School of Sciences and Engineering
in Partial Fulfillment of the Requirements for
the Degree of

Master of Science

in

Molecular Biology and Genetics

KOÇ
ÜNİVERSİTESİ

October 7, 2025

Production, Purification, and Crystallization Strategies for Recombinant EGFR and HER2 Tyrosine Kinase Domains as a Platform for Structure-Based Drug Discovery

Koç University

Graduate School of Sciences and Engineering

This is to certify that I have examined this copy of a master's thesis by

Edanur Topalan

and have found that it is complete and satisfactory in all respects,
and that any and all revisions required by the final
examining committee have been made.

Committee Members:

Assist. Prof. Hasan Demirci (Advisor)

Assoc. Prof. Halilibrahim Çiftçi (Co-Advisor)

Assoc. Prof. Belgin Sever

Assist. Prof. Onur Öztaş

Assist. Prof. İsmail Kudret Sağlam

Date: October, 7, 2025

[To my dear husband, Ufuk, my greatest supporter and best friend]

ABSTRACT

Production, Purification, and Crystallization Strategies for Epidermal Growth Factor Receptor (EGFR) and Human Epidermal Growth Factor Receptor 2 (HER2) Tyrosine Kinase Domains as a Platform for Structure-Based Drug Discovery

Edanur Topalan

Master of Science in Molecular Biology and Genetics

October 7, 2025

The epidermal growth factor receptor (EGFR) and human epidermal growth factor receptor 2 (HER2) tyrosine kinase domains (TKDs) are critical regulators of cell signaling and play central roles in cancer progression. Due to their therapeutic relevance, structural studies of EGFR-TKD and HER2-TKD are essential for structure-based drug discovery.

In this thesis, recombinant EGFR-TKD and HER2-TKD were produced, purified, and subjected to initial crystallization trials. Both genes were cloned into the pET28a(+) expression vector and expressed in *Escherichia coli (E. coli)*. Initial expression predominantly resulted in inclusion bodies; however, solubilization was successfully achieved using sarcosyl. Expression conditions, including temperature, inducer concentration, and induction time, were systematically optimized to improve yield and solubility. Purification strategies involved size-exclusion chromatography and a reverse affinity step to remove the SUMO tag, resulting in protein preparations suitable for crystallization.

Following optimization, soluble forms of both EGFR-TKD and HER2-TKD were obtained. Initial crystallization experiments yielded promising crystals for EGFR-TKD, while optimization of crystal quality for HER2-TKD is ongoing. These results establish robust production and purification workflows, providing structural platforms that can be used for future drug screening efforts and the development of novel inhibitors targeting EGFR and HER2.

ÖZETÇE

Epidermal Büyüme Faktörü Reseptörü (EGFR) ve İnsan Epidermal Büyüme Faktörü Reseptörü 2 (HER2) Tirozin Kinaz Domainlerinin İlaç Keşfine Yönelik Yapı-Temelli Çalışmalar İçin Üretim, Saflaştırma ve Kristalizasyon Stratejileri

Edanur Topalan

Moleküler Biyoloji ve Genetik, Yüksek Lisans

7 Ekim 2025

Epidermal büyüme faktörü reseptörü (EGFR) ve insan epidermal büyüme faktörü reseptörü 2 (HER2) tirozin kinaz domainleri (TKD), hücresel sinyal iletiminin kritik düzenleyicileridir ve kanser progresyonunda merkezi bir rol oynarlar. Bu nedenle, EGFR-TKD ve HER2-TKD'nin yapısal olarak incelenmesi, yapı-temelli ilaç keşfi çalışmalarında büyük önem taşımaktadır.

Bu tez kapsamında, rekombinant EGFR-TKD ve HER2-TKD'nin üretimi, saflaştırılması ve ilk kristalizasyon denemeleri gerçekleştirilmiştir. İlgili genler pET28a(+) ekspresyon vektörüne klonlanmış ve *Escherichia coli'*de eksprese edilmiştir. İlk denemelerde proteinlerin büyük kısmı inklüzyon cisimcikleri halinde elde edilmiştir; ancak sarkosil kullanımı ile başarılı bir şekilde çözünür hale getirilmiştir. Verim ve çözünürlüğü artırmak amacıyla sıcaklık, indükleyici konsantrasyonu ve indüksiyon süresi gibi koşullar optimize edilmiştir. Saflaştırma aşamalarında boyut-ayırma kromatografisi ve SUMO etiketinin uzaklaştırılması için ters afinite adımı kullanılmıştır. Bu yöntemlerle kristalizasyona uygun proteinler elde edilmiştir.

Optimizasyon sonrası her iki proteinin çözünür formları elde edilmiş, EGFR-TKD için ilk kristaller başarıyla büyütülmüş, HER2-TKD için ise kristal kalitesini artırmaya yönelik çalışmalar devam etmektedir. Bu sonuçlar, gelecekte yapılacak ilaç tarama çalışmaları ve yeni inhibitörlerin geliştirilmesi için güçlü yapısal platformlar sunmaktadır.

ACKNOWLEDGEMENTS

We often express our gratitude to everyone around us but forget to thank ourselves. Therefore, I would like to take a moment to acknowledge myself for the courage and perseverance I have shown throughout this journey. Despite my fears and doubts, I chose to move forward, and I am proud of what I have accomplished. I am also thankful to God for granting me the strength and opportunities that guided me along this path. This journey has not only been a scientific endeavor but also a personal one, where I learned to trust myself more deeply.

First and foremost, I would like to express my sincere gratitude to my advisor, Asst. Prof. Hasan DeMirci, and my co-advisor, Assoc. Prof. Halilibrahim Çiftçi, for giving me this opportunity, for their valuable guidance, and for their constant motivation and support throughout this journey. I am equally thankful to Assoc. Prof. Belgin Sever, who has always been ready to answer my questions and whose kindness and encouragement made the process much lighter.

I am deeply grateful to my family — my mother Sibel, my father Hakan, and my aunt Banu — for their endless love and encouragement. I also owe heartfelt thanks to my grandmother Emine and my grandfather İbrahim, who have always been a pillar of emotional support. Without them, this journey would have been much harder. To my brother Eymen, I want to say: may your path always be bright, and know that your sister will always be by your side.

Above all, I want to thank my husband Ufuk, *the love of my life*, who has walked beside me with endless patience, love, and faith. This journey would not have been the same without his constant encouragement and the warmth he brings to my life. *I love you.*

I am also grateful to all the members of KUYBIIGST-M — Alaleh Shafiei, Ayça İrgit, Bilge Tosun, Cahine Kulakman, Cengiz Kaan Ferah, Ebru Destan, Ece Akyüz, Fatma Betül Ertem, Haluk Çetinok, İlkin Yapıcı, Jerome Austin Johnson, Necati Atalay, Nilüfer Baldır, Ömür Güven, Seyide Seda Paydos, and Zeliş Nergis — for their friendship, kindness, and support. The moments we shared together made this journey not only more meaningful but also memorable. I would also like to thank Ahmet Büyükgüngör, Melih Çiğdem, and Sinan Güra for their valuable contributions to this work.

This study was supported by Scientific and Technological Research Council of Turkey (TUBITAK) under the Grant Number 122Z775 and Health Institutes of Türkiye (TUSEB) under the Grant Number 32988.The authors thank to TUBITAK and TUSEB for their supports. Co-funded by the European Union.

TABLE OF CONTENTS

LIST OF TABLES

LIST OF FIGURES

ABBREVIATIONS

AKT	Protein Kinase B
ATP	Adenosine Triphosphate
DNA	Deoxyribonucleic Acid
ECD	Extracellular Domain
EGF	Epidermal Growth Factor
EGFR	Epidermal Growth Factor Receptor
ERK	Extracellular Signal-Regulated Kinase
HER2	Human Epidermal Growth Factor Receptor 2
HER3	Human Epidermal Growth Factor Receptor 3
HER4	Human Epidermal Growth Factor Receptor 4
HDX-MS	Hydrogen–Deuterium Exchange Mass Spectrometry
IPTG	Isopropyl β-D-1-thiogalactopyranoside
JAK	Janus Kinase
kDa	Kilodalton
MAPK	Mitogen-Activated Protein Kinase
ml	Milliliter
mM	Millimolar
mTOR	Mechanistic Target of Rapamycin
Ni-NTA	Nickel–Nitrilotriacetic Acid
NSCLC	Non-Small Cell Lung Cancer
PBS	Phosphate-Buffered Saline
PCA	Principal Component Analysis
PDB	Protein Data Bank
PEG	Polyethylene Glycol
PKC	Protein Kinase C
PLCγ	Phospholipase C gamma
rpm	Revolutions per Minute
RTK	Receptor Tyrosine Kinase

SDS-PAGE	Sodium Dodecyl Sulfate Polyacrylamide Gel Electrophoresis
SEC	Size-Exclusion Chromatography
STAT	Signal Transducer and Activator of Transcription
SUMO	Small Ubiquitin-like Modifier
TGF-α	Transforming Growth Factor Alpha
TKD	Tyrosine Kinase Domain
XRD	X-ray Diffraction
µl	Microliter

Chapter 1:
INTRODUCTION

1.1 Receptor Tyrosine Kinases and the ErbB Family

Receptor tyrosine kinases (RTKs) constitute a large family of membrane proteins that regulate key cellular processes, including proliferation, survival, migration, and differentiation (Lemmon & Schlessinger, 2010; Hubbard, 1999; van der Geer, Hunter, & Lindberg, 1994). Within this family, the ErbB subgroup—EGFR (HER1/ErbB1), HER2 (ErbB2), HER3 (ErbB3), and HER4 (ErbB4)—plays a particularly important role in both normal physiology and tumorigenesis (Roskoski, 2014; Harris, 2003; Falls, 2003; Wilson et al., 2009).

EGFR was one of the earliest identified RTKs, and its study has shaped our understanding of cancer biology and targeted therapy development (Shi et al., 2010; Ferguson et al., 2003; Hubbard, 2004; Levantini et al., 2022). In contrast to EGFR, which is activated by ligands such as epidermal growth factor (EGF) and transforming growth factor-α (TGF-α) (Harris, 2003; Falls, 2003; Wilson et al., 2009), HER2 lacks a known ligand and instead functions as a preferred heterodimerization partner (Olayioye, 2000; Yarden & Pines, 2012). Through this role, HER2 strengthens and prolongs signaling, and its dysregulation is strongly associated with malignant transformation (Roskoski, 2014; Riudavets et al., 2021).

Activation of ErbB receptors triggers multiple downstream signaling pathways, including Ras/MAPK, PI3K/AKT/mTOR, PLCγ/PKC, and JAK/STAT, which regulate proliferation, metabolism, and survival. Aberrant activation of these cascades contributes to the development of aggressive tumors such as non-small cell lung cancer (NSCLC) and breast cancer. For this reason, EGFR and HER2 have emerged as major therapeutic targets and represent the central focus of this thesis.

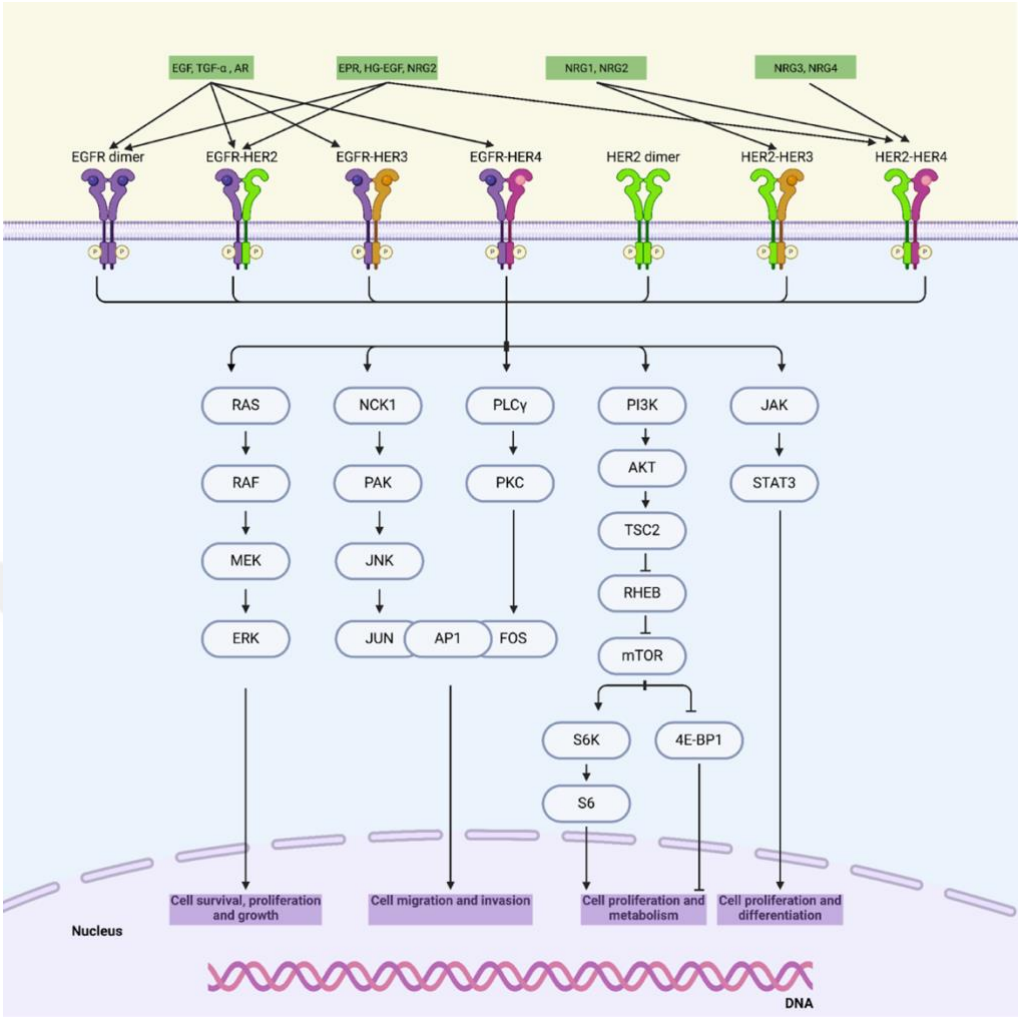

Figure 1.1: A general view of the pathway map of the ErbB family. Schematic representation of ErbB receptor-mediated signaling pathways. Ligand binding induces receptor homo- or heterodimerization, leading to phosphorylation of tyrosine residues in the intracellular kinase domains (shown as circled "P"). This phosphorylation recruits adaptor proteins and initiates several downstream cascades. In the Ras/Raf/MEK/ERK pathway, Grb2 and SOS activate RAS, which subsequently triggers RAF, MEK, and ERK activation. Nuclear ERK phosphorylates transcription factors such as ELK1, promoting gene expression linked to proliferation and survival. The PI3K/AKT/mTOR pathway is activated by membrane-associated PI3K, which converts PIP2 to PIP3 and leads to AKT activation. AKT phosphorylates multiple substrates, including TSC2, which enhances mTOR activity and promotes protein synthesis and cell growth. In the PLCγ/PKC pathway, PLCγ generates DAG and IP3 from PIP2; DAG activates PKC, which regulates transcription factors such as FOS. The JAK/STAT3 pathway involves phosphorylation

and dimerization of STAT3 by JAK kinases, enabling nuclear translocation and transcription of genes associated with survival and differentiation. Finally, the NCK1/PAK/JNK cascade connects receptor activation to phosphorylation of c-JUN by JNK, which forms the AP-1 complex and regulates genes linked to migration and invasion. Figure created with BioRender. (Topalan et al., 2025)

1.2 Structural Features of EGFR and HER2

EGFR and HER2 share a conserved architecture characteristic of ErbB family receptors. Both proteins consist of an extracellular ligand-binding domain (ECD), a single transmembrane segment, a juxtamembrane region, an intracellular tyrosine kinase domain (TKD), and a C-terminal tail (Zhang et al., 2006; Lemmon et al., 2014; Yarden & Sliwkowski, 2001). In EGFR, ligand binding to the extracellular domain induces conformational rearrangements that expose a dimerization arm, thereby promoting homo- or heterodimerization (Cho et al., 2003; Ogiso et al., 2002). In contrast, HER2 is maintained in a conformation that is constitutively competent for dimerization, even in the absence of a ligand, which explains its role as the preferred dimerization partner within ErbB signaling networks (Olayioye, 2000; Roskoski, 2014)

The intracellular TKDs of both receptors contain the canonical elements required for kinase activity, including the ATP-binding cleft, the activation loop, and conserved motifs that regulate catalytic function. Structural studies of EGFR-TKD have described distinct conformational states. In the inactive state, the activation loop folds into a short helix and the αC helix is displaced outward, whereas in the active state, the activation loop extends and the αC helix rotates inward, properly aligning catalytic residues for ATP binding and substrate phosphorylation (Yun et al., 2007; Jura et al., 2009).

HER2-TKD maintains the same general topology but exhibits greater conformational flexibility. Crystallographic analyses have shown that this structural plasticity complicates the development of selective inhibitors, as the kinase domain can assume multiple orientations of the activation loop and regulatory motifs (Aertgeerts et al., 2011;

Morrow & Grant, 2000). This flexibility is thought to contribute to the difficulty of designing inhibitors that specifically target HER2 without affecting other ErbB family members (Riudavets et al., 2021; Zhao et al., 2021).

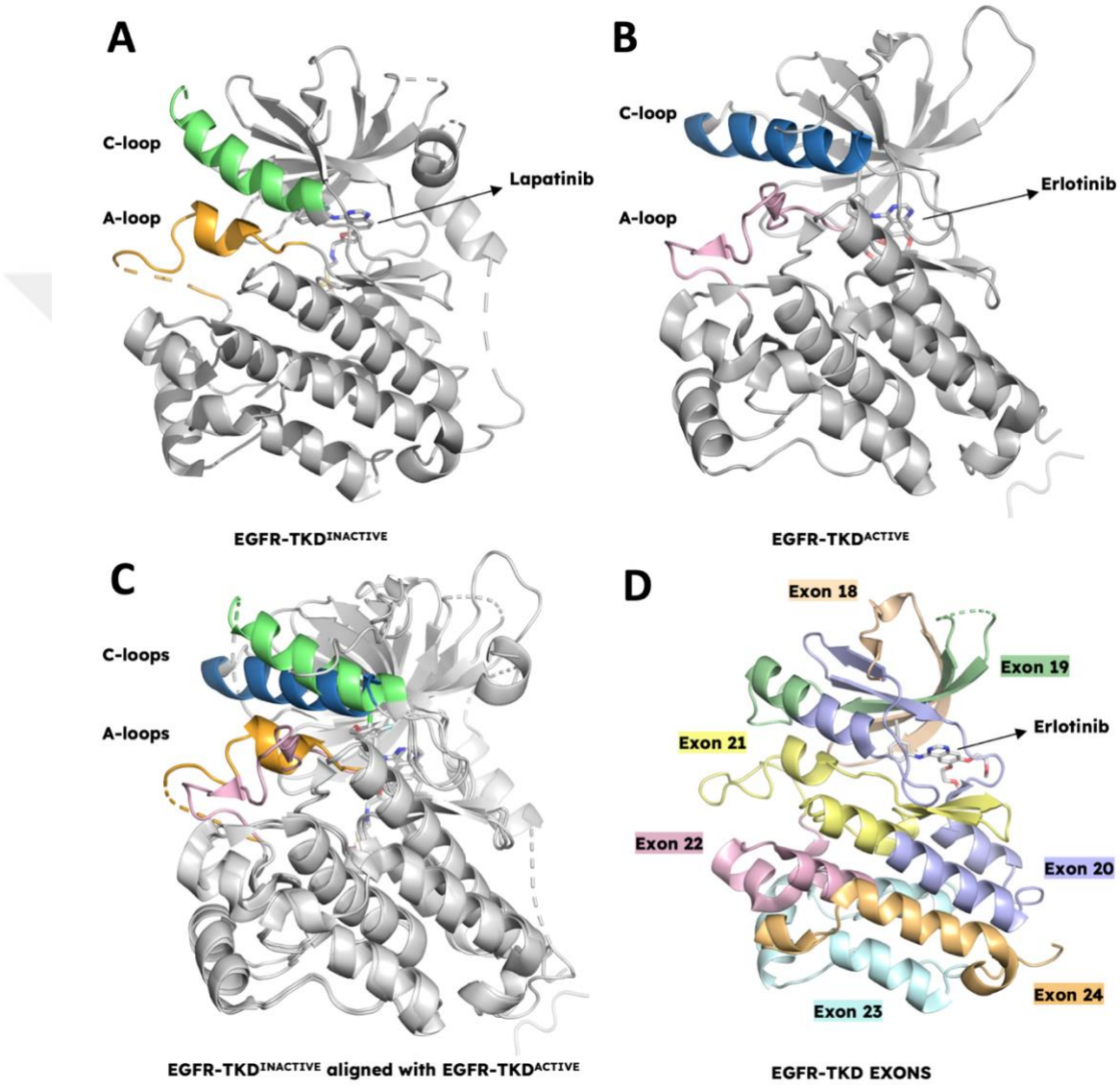

Figure 1.2: Structural features of the EGFR tyrosine kinase domain (TKD). **(A)** Inactive conformation of EGFR-TKD bound to lapatinib (PDB: 1XKK), showing the helical turn within the activation loop (orange) and the outward orientation of helix αC (green). **(B)** Active conformation of EGFR-TKD bound to erlotinib (PDB: 1M17), characterized by an extended activation loop (orange) and inward rotation of helix αC (green). **(C)** Superimposition of inactive and active EGFR-TKD conformations highlights conformational switching. **(D)** Exon map of EGFR-TKD, color-coded from exon 18

(wheat) through exon 24 (orange), using the erlotinib-bound structure (PDB: 4HJO). Structural models were prepared with PyMOL (Schrödinger LLC). (Topalan et al., 2025)

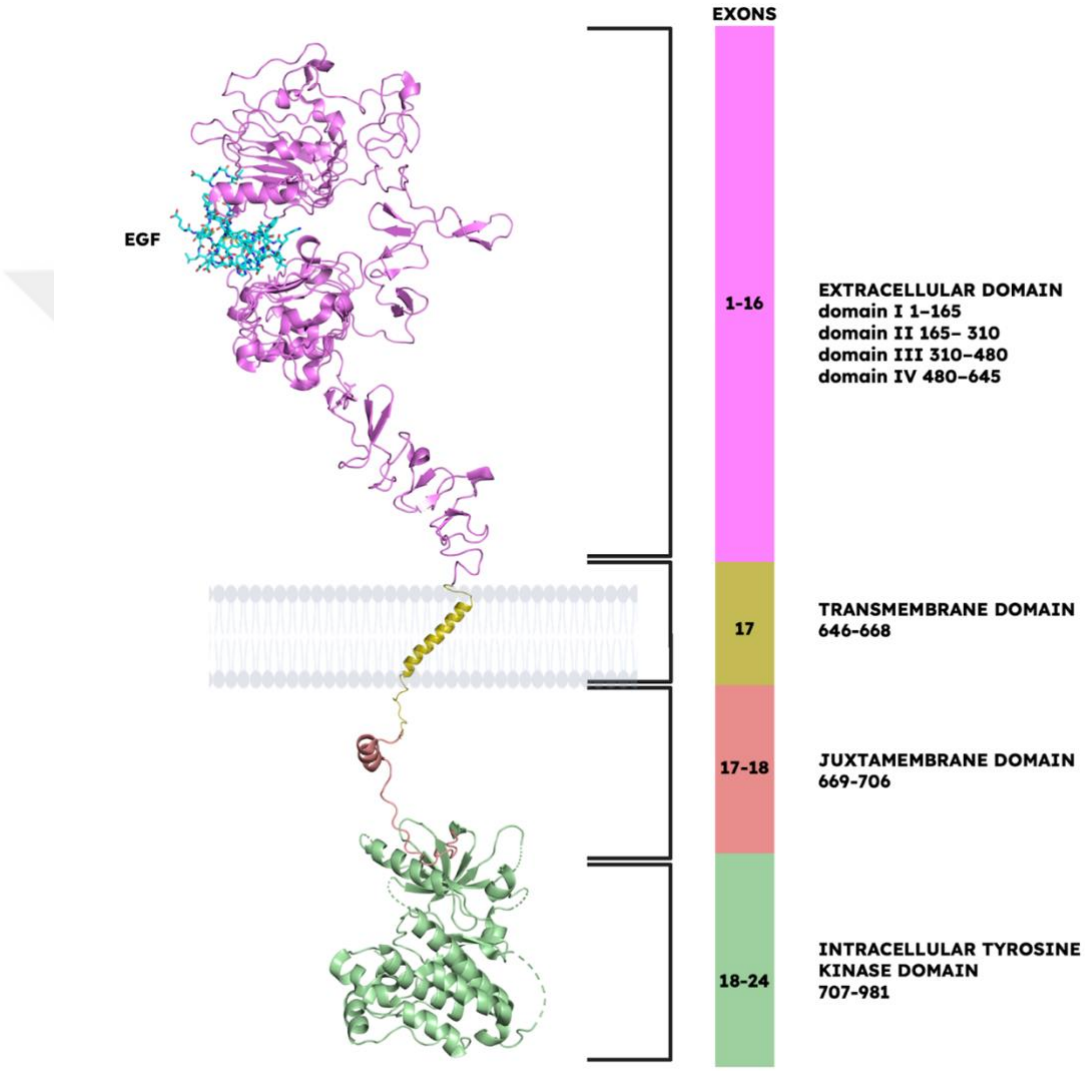

Figure 1.3: An overview of the EGFR structure. The figure illustrates a schematic representation of the epidermal growth factor receptor (EGFR) structure. The diagram highlights the extracellular domain (ECD, PDB: 3NJP), transmembrane domain (TMD, PDB: 2KS1), juxtamembrane domain (JMD, PDB: 3GOP), and intracellular tyrosine kinase domain (TKD, PDB: 3GOP). Figure created using PyMOL (PyMOL Molecular Graphics System, Version 3.0, Schrödinger LLC). (Topalan et al., 2025)

1.3 Oncogenic Mutations in NSCLC

Non-small cell lung cancer (NSCLC) is the predominant subtype of lung cancer, comprising nearly 85% of cases worldwide, and remains one of the leading causes of cancer-related mortality (Mok et al., 2009). Among the main oncogenic drivers of NSCLC are mutations in the EGFR gene. The most frequent alterations are exon 19 deletions and the L858R point mutation in exon 21, which together account for approximately 85–90% of EGFR-mutant cases (Pao & Chmielecki, 2010; Westover et al., 2018; Nilsson et al., 2021). These mutations enhance kinase activity, leading to sustained downstream signaling and uncontrolled proliferation.

Alterations in HER2 have also been identified in NSCLC and other malignancies. Gene amplification and exon 20 insertions, in particular, are established oncogenic events that drive aberrant signaling and are often associated with poor prognosis (Li et al., 2020; Oxnard et al., 2013; Yu et al., 2023; Riudavets et al., 2021). Mutations affecting both EGFR and HER2 therefore represent critical molecular targets, highlighting the importance of developing selective therapeutic strategies against these receptors.

1.4 Therapeutic Strategies and Resistance Mechanisms

Identification of EGFR and HER2 as key oncogenic drivers has enabled the development of a variety of targeted therapies. For EGFR, the first-generation tyrosine kinase inhibitors (TKIs) gefitinib and erlotinib initially provided clear clinical benefit. However, their effect was often short-lived due to the rapid emergence of resistance mutations, most notably the T790M substitution (Kobayashi et al., 2005). Second-generation irreversible TKIs, such as afatinib and dacomitinib, were designed to overcome this limitation by broadly inhibiting the ErbB family, but their use was restricted by dose-limiting toxicities (Sequist et al., 2013). More recently, third-generation inhibitors such as osimertinib were developed to selectively target T790M

while sparing wild-type EGFR, and these agents have become standard treatments in clinical practice (Soria et al., 2018).

In the case of HER2, both monoclonal antibodies and small molecules are employed. Trastuzumab, along with antibody–drug conjugates such as trastuzumab emtansine and trastuzumab deruxtecan, represent important components of HER2-targeted therapy. In addition, small-molecule TKIs including neratinib and poziotinib have expanded therapeutic options for HER2-driven cancers (Moasser, 2007; Zhou et al., 2020).

Despite these advances, resistance remains a major challenge. Mechanisms include secondary kinase domain mutations (e.g., EGFR C797S, HER2 exon 20 insertions), activation of alternative signaling pathways, and phenotypic adaptations such as epithelial-to-mesenchymal transition (Yu et al., 2013). These processes reduce long-term treatment efficacy and emphasize the ongoing need for next-generation inhibitors and rational combination strategies.

Table 1.1: FDA-approved small-molecule tyrosine kinase domain inhibitors (TKI) of EGFR (Topalan et al., 2025). Three generations of TKIs, as well as their molecular target of inhibition are illustrated in the table, each one with a different color code (1st generation: green; 2nd generation: blue; 3th generation: yellow). The 4th generation of EGFR-TKIs are currently undergoing preclinical evaluation, and therefore are not present in the table.

Inhibitor Name	Generation & Mode of Action	Molecular Target	Tumor Type
Erlotinib	1st Reversible, Competitive	ATP binding site of EGFR TKD	Locally advanced or metastatic NSCLC, pancreatic cancer
Gefitinib	1st Reversible, Competitive	ATP binding site of EGFR TKD	Advanced or metastatic NSCLC, pancreatic cancer
Lapatinib	1st Reversible, Competitive	ATP binding site of EGFR & HER2 TKD	Metastatic breast cancer, gastric cancer
Icotinib	1st Reversible, Competitive	ATP binding site of EGFR TKD	Advanced or metastatic NSCLC
Dacomitinib	2nd Covalently binding, irreversible	ATP binding site of EGFR, HER2, and HER4	Metastatic NSCLC
Afatinib	2nd Covalently binding, irreversible	ATP binding site of EGFR, HER2, and HER4	Metastatic NSCLC, breast cancer
Neratinib	2nd Covalently binding, irreversible	ATP binding site of EGFR, HER2, and HER4	Breast cancer
Brigatinib	2nd Covalently binding, irreversible	ATP binding site of EGFR TKD	NSCLC, anaplastic large cell lymphoma, neuroblastomas
Osimertinib	3th Covalently binding, irreversible	ATP binding site of the EGFR	Advanced and metastatic NSCLC
Lazertinib	3th Covalently binding, irreversible	ATP binding site of the EGFR	Advanced NSCLC
Furmonertinib	3th Covalently binding, irreversible	ATP binding site of the EGFR	Locally advanced or metastatic NSCLC

1.5 X-ray Crystallography in Structural Biology

The three-dimensional structures of proteins at atomic resolution can be determined by several biophysical methods, including nuclear magnetic resonance (NMR), cryo-electron microscopy (cryo-EM), and X-ray crystallography. Among these, X-ray crystallography remains the most widely used technique, providing detailed structural information that has been central to modern biology and drug discovery (Smyth & Martin, 2000).

A typical crystallographic workflow includes the growth of high-quality protein crystals, collection of diffraction data upon X-ray exposure, determination of phases, calculation of electron density maps, model building, and final refinement and validation (Mishra et al., 2012). Each of these steps is highly interdependent, and limitations at one stage can compromise the accuracy of the final structure.

Protein crystallization is often the most challenging step and frequently represents the major bottleneck in the process. Successful crystallization strongly depends on protein-related factors such as purity, concentration, solubility, homogeneity, and stability (Chayen & Saridakis, 2008; Holcomb et al., 2017). High purity is usually obtained through sequential chromatographic methods, including affinity, ion-exchange, and size-exclusion chromatography (Giegé et al., 1995; McPherson & Gavira, 2014).

Protein concentration also plays a critical role: insufficient concentrations hinder nucleation, while excessively high concentrations promote aggregation or poorly ordered crystals (Weber, 1991). A proper balance between solubility and supersaturation must be maintained, as highly soluble proteins resist nucleation whereas poorly soluble proteins tend to precipitate.

Additional difficulties arise from the inherent flexibility of many proteins. Flexible loops, unstable domains, or heterogeneous oligomeric states can disrupt crystal lattice formation, while even minor heterogeneities such as post-translational modifications may compromise crystal quality (Holcomb et al., 2017).

Finally, the crystallization environment (including pH, salt concentration, and precipitant type) has a strong influence on nucleation and packing. To address this complexity, systematic screening across hundreds of conditions is routinely employed in structural biology laboratories (Weber, 1991).

1.6 Motivation and Aim

The dysregulation of EGFR and HER2 is a major factor in the onset and progression of NSCLC. Although targeted therapies against these receptors have improved clinical outcomes, resistance mutations frequently emerge and limit long-term effectiveness. Addressing this issue requires structural studies that can guide the design of inhibitors with greater potency and selectivity.

Recombinant production of the tyrosine kinase domains (TKDs) of EGFR and HER2 provides the foundation for such structural investigations. However, both proteins are difficult to obtain in soluble form, as they typically accumulate in inclusion bodies when expressed in bacterial systems. Previous studies, including our own work, have applied solubilization approaches such as sarcosyl-assisted lysis and modified purification protocols, along with initial crystallization trials, to address these challenges. In parallel, efforts within our group have focused on the development of small-molecule scaffolds such as pyrazoline–thiazole hybrids, which have shown promising inhibitory activity against EGFR in preclinical models.

The aim of this thesis is twofold: first, to optimize expression and purification strategies for recombinant EGFR-TKD and HER2-TKD in *E. coli*; and second, to establish preliminary crystallization conditions to enable future structural studies. These efforts are expected to provide the groundwork for detailed structural characterization and support the rational design of next-generation inhibitors targeting resistant variants in NSCLC.

Chapter 2:
MATERIALS AND METHODS

2.1 Materials and Equipment

2.1.1 Stock solutions and LB medium

LB medium (Table 2.1) and stock solutions of antibiotics and 0.4 M IPTG (Table 2.2) were prepared to be used in transformation and protein expression experiments.

Table 2. 1: LB Medium

Reagent	**Amount (g/L)**
Tryptone	10
NaCl	10
Yeast extract	5
Total	25

Table 2. 2: Antibiotics and 0.4 M IPTG Stock Solutions

Reagent	**Amount (mg/ml)**
Kanamycin	50
Chloramphenicol	35
IPTG	95.324

2.1.2 Buffers

For small-scale expression check and protein purification, lysis buffers (Table 2.3), Ni-NTA affinity chromotogrpahy purification buffers (Table 2.4), and SEC buffer (Table 2.5) were prepared

Table 2. 3: Lysis Buffers

Triton X-100 Lysis Buffer Reagents	**Final concentration**
NaCl	150 mM
Tris-HCl	50 mM
Imidazole	20 mM
Glycerol	5% (v/v)
Triton X-100	0.5% (v/v)
PMSF	1 mM
β-ME	5 mM
Sarcosyl Lysis Buffer Reagents	**Final concentration**
NaCl	150 mM
Tris-HCl	10 mM
PMSF	1 mM
β-ME	5 mM
Sarcosyl	1.5% (m/v)

Table 2. 4: Purification Buffers

His A Buffer Reagents	**Final concentration**
NaCl	150 mM
Tris-HCl	20 mM
Glycerol	5% (v/v)
His B Buffer Reagents	**Final concentration**
NaCl	150 mM
Tris-HCl	20 mM
Imidazole	250 mM
SEC Buffer Reagents	**Final concentration**
NaCl	150 mM
Tris-HCl	20 mM

2.2 Gene Design and Cloning

2.2.1 Construction of EGFR-TKD Expression Vector

The coding sequence of the Epidermal Growth Factor Receptor Tyrosine Kinase Domain (EGFR-TKD), shown below, was cloned into the pET-28a(+) expression vector. The construct was designed to include an N-terminal 6×His-SUMO tag containing a ULP1 protease cleavage site. The *NdeI* and *BamHI* restriction sites were used for cloning, and the kanamycin resistance gene served as the selection marker. The resulting recombinant plasmid was transformed into *E. coli* BL21 Rosetta-2 competent cells using the heat-shock method.

EGFR-TKD amino acid sequence (SUMO tag in bold):

MSDSEVNQEAKPEVKPEVKPETHINLKVSDGSSEIFFKIKKTTPLRRLM EAFAKRQGKEMDSLRFLYDGIRIQADQTPEDLDMEDNDIIEAHREQIGGGA MGIRSGEAPNQALLRILKETEFKKIKVLGSGAFGTVYKGLWIPEGEKVKIPVAIK ELREATSPKANKEILDEAYVMASVDNPHVCRLLGICLTSTVQLITQLMPFGCLL DYVREHKDNIGSQYLLNWCVQIAKGMNYLEDRRLVHRDLAARNVLVKTPQH VKITDFGLAKLLGAEEKEYHAEGGKVPIKWMALESILHRIYTHQSDVWSYGVT VWELMTFGSKPYDGIPASEISSILEKGERLPQPPICTIDVYMIMVKCWMIDADSR PKFRELIIEFSKMARDPQRYLVIQGDERMHLPSPTDSNFYRALMDEEDMDDVV DADEYLIPQQG* (PDB ID: 3VJO)

2.2.2 Construction of HER2-TKD Expression Vector

The coding region of the human HER2 tyrosine kinase domain (HER2-TKD) was cloned into the pET-28a(+) expression vector. The construct contained an N-terminal 6×His tag to facilitate purification and a SUMO tag to improve solubility, including a ULP1 protease cleavage site for subsequent removal. The kanamycin resistance gene of

the plasmid served as the selection marker. The final recombinant vector was used for transformation into *E. coli* host cells.

HER2-TKD amino acid sequence (SUMO tag in bold):

MSDSEVNQEAKPEVKPEVKPETHINLKVSDGSSEIFFKIKKTTPLRRLM EAFAKRQGKEMDSLRFLYDGIRIQADQTPEDLDMEDNDIIEAHREQIGGMS GAAPNQALLRILKETELRKVKVLGSGAFGTVYKGIWIPDGENVKIPVAIKVLRE NTSPKANKEILDEAYVMAGVGSPYVSRLLGICLTSTVQLVTQLMPYGCLLDHV RENRGRLGSQDLLNWCMQIAKGMSYLEDVRLVHRDLAARNVLVKSPNHVKIT DFGLARLLDIDETEYHADGGKVPIKWMALESILRRRFTHQSDVWSYGVTVWEL MTFGAKPYDGIPAREIPDLLEKGERLPQPPICTIDVYMIMVKCWMIDSECRPRFR ELVSEFSRMARDPQRFVVIQNEDLGPASPLDSTFYRSLLEDDDMGDLVDAEEYL VPQQGAAAS* (PDB ID: 3RCD)

2.3 Bacterial Transformation and Colony Selection

For both EGFR-TKD and HER2-TKD constructs, transformation was carried out in *E. coli* BL21 Rosetta-II competent cells using the standard heat-shock method.

For EGFR-TKD, 50 µL of competent cells were gently mixed with 2 µL of plasmid DNA and kept on ice for 20 minutes. Heat shock was applied at 42 °C for 45 seconds, followed by immediate cooling on ice for 2 minutes. Cells were then resuspended in 500 µL antibiotic-free LB medium and incubated at 37 °C for 90 minutes with gentle shaking. After a short centrifugation (1500 rpm, 2 minutes), the pellet was resuspended in the residual LB medium and spread onto LB agar plates containing kanamycin (50 µg/mL) and chloramphenicol (35 µg/mL). Plates were incubated overnight at 37 °C to allow colony formation.

For HER2-TKD, a similar procedure was followed. 2 µg of plasmid DNA was dissolved in 25 µL distilled water, vortexed, and briefly centrifuged at 9000 rpm for 4 minutes to ensure homogeneity. 2 µL of this plasmid preparation was added to 50 µL of Rosetta-II competent cells, followed by incubation on ice for 20 minutes. Heat shock was applied at 42 °C for 45 seconds, then cells were transferred to ice for 2 minutes. Following recovery in 500 µL sterile LB medium at 37 °C for 90 minutes with gentle mixing, 50 µL of the culture was plated on LB agar containing kanamycin (50 µg/mL) and chloramphenicol (35 µg/mL). Plates were incubated overnight at 37 °C.

The next day, individual colonies from both EGFR-TKD and HER2-TKD transformation plates were picked and inoculated into 7–10 mL LB broth containing the corresponding antibiotics. Cultures were grown at 37 °C, 110 rpm overnight, and turbidity was used as confirmation of successful bacterial growth. For long-term storage, 750 µL of the overnight culture was mixed with 750 µL of sterile 80% glycerol in cryotubes, vortexed gently to ensure homogeneity, and stored at −80 °C as glycerol stocks.

2.4 Expression and Solubility Screening

2.4.1 Experimental Design and Assessment Parameters

Mini-scale experiments were carried out primarily with EGFR-TKD to determine optimal conditions for expression and solubility prior to scale-up production. The parameters evaluated included IPTG concentration (0.05–0.40 mM), induction temperature (16 °C, 30 °C, and 37 °C), and induction duration (1–8 h, 16 h at 37 °C, and overnight at 16–18 °C). Different host strains were also tested, including Rosetta-II, BL21 Star, and C43, to assess strain-dependent effects on protein recovery. Lysis buffer conditions were varied with respect to pH (7.5–8.5), NaCl concentration (50–1000 mM), $MgCl_2$ (5 mM), β-mercaptoethanol (1–5 mM), and imidazole (10–20 mM where applicable). Detergent-based lysis was compared between Triton X-100 (0.1–2.5%) and sarcosyl (0.1–1.5%). In addition, a urea gradient (0–8 M) was tested for solubilization of inclusion bodies. Expression and solubility under these conditions were analyzed by SDS-

PAGE of before-induction (BI), whole-cell lysate (WCL), pellet, supernatant, and Ni-NTA pull-down samples.

For HER2-TKD, mini-scale assays focused on a narrower set of parameters. Cultures were induced at 37 °C with 0.4 mM IPTG, and expression was monitored across different induction times (1–8 h and 16 h). Solubility was evaluated using Triton X-100– and sarcosyl-based lysis buffers. SDS-PAGE analysis of WCL, pellet, and supernatant fractions was performed to assess protein recovery.

2.4.2 EGFR-TKD: Mini-Scale Expression and Solubility

For the initial evaluation of EGFR-TKD expression, small-scale cultures were induced with 0.4 mM IPTG and incubated either overnight at 16 °C and 30 °C, or for 4 h at 37 °C. Cells were collected by centrifugation at 6000 rpm for 5 min at 4 °C and resuspended in lysis buffer containing 50 mM Tris-HCl (pH 8.0), 150 mM NaCl, 5 mM $MgCl_2$, 1 mM PMSF, 5 mM β-mercaptoethanol, 5% glycerol, and Triton X-100 (0.5%). Cell disruption was performed by sonication, and the lysates were clarified by centrifugation. Pellet and supernatant fractions were analyzed by SDS-PAGE.

To assess solubility, mini-scale Ni-NTA pull-down experiments were performed using 40 µL of beads. The beads were washed with HisA buffer (150 mM NaCl, 20 mM Tris-HCl, 10 mM imidazole, 5% glycerol, pH 8.0) and eluted with HisB buffer (200 mM NaCl, 20 mM Tris-HCl, 250 mM imidazole, 5% glycerol, pH 8.0).

Further solubilization strategies were tested. Lysis buffers containing either Triton X-100 or 1.5% sarcosyl were compared. In addition, a urea gradient (0–8 M; 50 mM Tris-HCl pH 7.5, 500 mM NaCl, 20 mM imidazole, 5% glycerol) was applied to inclusion body preparations to evaluate denaturation-based recovery. Whole-cell lysates, pellets, supernatants, and eluates were analyzed by SDS-PAGE to monitor expression and solubility under each condition.

2.4.3 HER2-TKD: Mini-Scale Expression and Solubility

For HER2-TKD, cultures were induced with 0.4 mM IPTG at 37 °C and sampled at different induction times (1–8 h and 16 h). Cells were harvested by centrifugation (6000 rpm, 5 min, 4 °C), resuspended in lysis buffer, and disrupted by sonication. Lysates were clarified, and pellet and supernatant fractions were analyzed by SDS-PAGE.

Detergent-based solubility screening was performed using two different lysis conditions: a Triton X-100–based buffer (200 mM NaCl, 20 mM imidazole, 50 mM Tris-HCl, 5% glycerol, pH 8.5) and a sarcosyl-based buffer (10 mM Tris-HCl pH 8.5, 150 mM NaCl, 1 mM PMSF, 5 mM β-mercaptoethanol, 1.5% sarcosyl). Fractions from both preparations, including WCL, pellet, and supernatant, were subjected to SDS-PAGE for evaluation of protein expression and solubility.

2.4.4 Host Strain Evaluation for EGFR-TKD

EGFR-TKD constructs were transformed into *E. coli* BL21 C43, and Gami-II strains in addition to Rosetta-II. For mini-scale expression trials, single colonies were inoculated and induced under the same IPTG concentration, temperature, and incubation time as previously optimized. Cell pellets were resuspended in Triton X-100–based lysis buffer (50 mM Tris-HCl pH 8.0, 50 mM NaCl, 5 mM $MgCl_2$, 1 mM PMSF, 1 mM β-mercaptoethanol, 5% glycerol, 0.5% Triton X-100) and disrupted by sonication. Lysates were clarified by centrifugation, and samples from whole-cell lysate, pellet, and supernatant fractions were analyzed by SDS-PAGE. Mini Ni-NTA pull-down assays were also performed to assess the solubility of the expressed protein across the different strains.

2.5 Large-Scale Expression of Recombinant Proteins

2.5.1 Large-Scale Production of EGFR-TKD

For large-scale protein production, *E. coli* Rosetta-II glycerol stocks carrying the EGFR-TKD construct were used. LB medium (50 g/L) was prepared and autoclaved at 121 °C for 20 min. After cooling, kanamycin (50 µg/mL) and chloramphenicol (35 µg/mL) were added as selective antibiotics. A 50 mL starter culture was inoculated and incubated overnight at 37 °C with shaking at 110 rpm.

The overnight culture was transferred into 1 L LB medium supplemented with the same antibiotics. Cell growth was monitored by measuring OD_{600} using a NanoDrop spectrophotometer. When OD_{600} reached 0.6–0.8, protein expression was induced with 0.4 mM IPTG. Cultures were incubated at 37 °C, 110 rpm, for 4 h. Cells were harvested by centrifugation at 3500 rpm for 45 min at 4 °C, and pellets were collected. The supernatant was discarded, and the pellets were stored at −45 °C until further use.

2.5.2 Large-Scale Production of HER2-TKD

Following the optimization of induction time and solubilization conditions, large-scale expression of HER2-TKD was performed. Four 1 L LB cultures were grown at 37 °C until the optical density at 600 nm (OD_{600}) reached ~0.6. Protein expression was induced with 0.4 mM IPTG, and cultures were incubated for an additional 7 h at 37 °C. Cells were harvested by centrifugation at 3500 rpm for 45 min at 4 °C, and the resulting pellets were stored at −45 °C until further processing.

For lysis, the cell pellets were resuspended in 10 mM Tris-HCl (pH 8.5), 150 mM NaCl, 1 mM PMSF, 5 mM β-mercaptoethanol (BME), and 1.5% (w/v) sarcosyl. Sonication was carried out at 41% amplitude in 11 cycles of 20 s on ice, until the viscosity of the suspension was visibly reduced. Lysates were clarified by ultracentrifugation at 35,000 rpm for 1 h at 4 °C. To minimize detergent carry-over, the supernatant was

dialyzed overnight at 4 °C against 2 × 1 L of dialysis buffer (0.1% Triton X-100) using a suitable molecular weight cut-off membrane.

Following dialysis, the clarified supernatant was applied to a nickel–nitrilotriacetic acid (Ni-NTA) affinity column equilibrated with HisA buffer. Bound proteins were eluted with HisB buffer. Fractions from each purification step were collected and analyzed by SDS-PAGE.

Buffers used during purification:

HisA buffer: 150 mM NaCl, 20 mM Tris-HCl, 5% glycerol, pH 8.0

HisB buffer: 150 mM NaCl, 20 mM Tris-HCl, 250 mM imidazole, 5% glycerol, pH 8.0

2.6 Protein Purification and Tag Removal

2.6.1 Purification and Tag Removal of EGFR-TKD

The bacterial cells were resuspended in a lysis buffer containing 10 mM Tris (pH 8.0), 150 mM NaCl, 1 mM PMSF, 5 mM β-mercaptoethanol (BME), and 1.5% Sarkosyl. Cell lysis was carried out using a Branson W250 sonicator (Brookfield, CT, USA). The resulting lysate was ultracentrifuged at 35,000 rpm for 45 minutes at 4 °C using a Ti-45 rotor in a Beckman Optima™ L-80 XP ultracentrifuge (Beckman, USA). The insoluble fraction was discarded, and the clarified supernatant was loaded onto a Superdex 200 size-exclusion chromatography column at a flow rate of 1 mL/min. Fractions were collected every 5 mL, and samples were taken for SDS-PAGE analysis to assess purity and molecular weight. Equilibration and washing were performed using a buffer containing 150 mM NaCl and 20 mM Tris-HCl (pH 8.0).

The eluted EGFR-TKD protein was subjected to cleavage tests to determine optimal conditions for removing the N-terminal SUMO tag using ULP1 protease. The efficiency of cleavage was assessed by testing different ULP1-to-protein ratios (1:1000 and 5:100), incubation temperatures (4 °C, 37 °C, and room temperature), and time points (30 min, 1 h, 2 h, 4 h, and overnight). Based on these tests, the optimal condition was selected. The eluted protein was then dialyzed at 4 °C for 30 minutes using a 3 kDa cut-off membrane in the washing buffer (150 mM NaCl and 20 mM Tris-HCl, pH 8.0) supplemented with 5:1000 ULP1 protease to ensure efficient SUMO tag removal. To separate tag-free EGFR-TKD from the cleaved SUMO fragment and residual tagged protein, the sample was passed through a Ni-NTA column, where the untagged protein was collected in the flow-through. The purified EGFR-TKD was subsequently concentrated to 2.4 mg/mL using Millipore ultrafiltration columns and stored at −80 °C for crystallization trials.

2.6.2 Purification and Tag Removal of HER2-TKD

Size-exclusion chromatography (SEC) was performed to further purify HER2-TKD. The protein sample was loaded onto a Superdex-200 column equilibrated with buffer containing 150 mM NaCl and 20 mM Tris-HCl (pH 8.0). Elution was monitored by UV absorbance, and fractions of 5 mL were collected. SDS-PAGE analysis showed that fractions 9–13 contained the highest amounts of HER2-TKD, which were subsequently pooled and concentrated using 30 kDa Amicon centrifugal filters (2500 rpm, 15 min, three rounds).

Tag removal was performed by incubating the concentrated HER2-TKD with ULP protease (5:1000, w/w) at 4 °C for 40 min. The reaction mixture was then passed through a Ni-NTA column to separate the cleaved HER2 protein from the His_6-SUMO tag and any uncleaved protein.

The buffers used during these steps were:

HisA buffer: 150 mM NaCl, 20 mM Tris-HCl, 5% glycerol, pH 8.0

HisB buffer: 150 mM NaCl, 20 mM Tris-HCl, 250 mM imidazole, 5% glycerol

At each stage, flow-through and elution fractions were collected, and representative samples (including pre-cleavage controls) were analyzed by SDS-PAGE to confirm the efficiency of tag removal and overall purification.

2.7 Crystallization Trials of EGFR and HER2

2.7.1 Screening of Crystallization Conditions for EGFR-TKD

Crystallization experiments for EGFR-TKD were carried out using the microbatch-under-oil method in 72-well Terasaki plates. Both apo EGFR-TKD and complexes with small-molecule inhibitors (Erlotinib, Lapatinib, and B2) were tested. Prior to crystallization, the protein samples were purified by size-exclusion chromatography (SEC). In some preparations, the His_6-SUMO tag was removed by ULP1 cleavage and separated by reverse Ni-NTA chromatography, while in others the tagged protein was directly used for screening. Protein concentrations were adjusted according to the peak fractions obtained from SEC, and β-mercaptoethanol was included in selected trials.

For each well, 0.83 µL protein solution was mixed with an equal volume of reservoir solution taken from commercial sparse-matrix screens, and the drops were sealed under 16.6 µL paraffin oil. In total, approximately 3000 different crystallization conditions were tested. Trials were performed in parallel at 4 °C and at room temperature. The plates were inspected regularly by light microscopy. In cases where microcrystals or weakly diffracting crystals were observed, optimization was attempted by varying the protein-to-reservoir ratios (e.g., 0.70–1.25 µL reservoir against 0.83 µL protein) while keeping other parameters constant.

Preliminary X-ray screening was conducted both in situ and after crystal harvesting. Data collection was performed at the Turkish Light Source using a Rigaku XtaLAB Synergy Flow diffractometer equipped with an XtalCheck-S plate reader. For room-temperature measurements, an Oxford Cryosystems Cryostream 800 Plus was used, set to 300 K.

2.7.2 Screening of Crystallization Conditions for HER2-TKD

Crystallization trials for HER2-TKD were performed using the microbatch-under-oil method in 72-well Terasaki plates, following a workflow similar to that used for EGFR-TKD. Both apo protein samples and complexes with small-molecule inhibitors (B2) were included in the screening. Prior to crystallization, the protein was purified by size-exclusion chromatography (SEC). In most preparations, the His_6-SUMO tag was removed by ULP1 protease and separated by reverse Ni-NTA chromatography; in a few trials, SUMO-tagged protein was directly tested.

Each crystallization drop consisted of 0.83 µL protein solution mixed with 0.83 µL reservoir solution from commercial sparse-matrix screens, and overlaid with 16.6 µL paraffin oil. The experiments were conducted in parallel at 4 °C and at room temperature. Plates were inspected regularly by light microscopy to monitor crystal formation. In cases where microcrystals or initial precipitation patterns were observed, optimization was attempted by adjusting the protein-to-reservoir ratios under the same buffer conditions.

2.7.3 Optimization of Crystal Growth and X-ray Screening

Initial conditions that produced crystalline material or weakly diffracting samples were selected for further optimization. Parameters such as pH, precipitant type and concentration (for example, different PEG variants and salts including lithium sulfate or potassium thiocyanate), and buffer systems (e.g., HEPES, Bis-Tris) were systematically

varied. In addition, drop-ratio experiments were performed to balance nucleation and crystal growth.

Crystals were monitored by light microscopy and, when suitable, were tested for diffraction quality. Screening was carried out either directly in the crystallization plates or after crystal harvesting. Room-temperature diffraction experiments were performed using a Rigaku XtaLAB Synergy Flow diffractometer equipped with an XtalCheck-S plate reader. When indicated, crystals were cryoprotected using standard protocols and tested under cryogenic conditions. Diffraction images were processed using CrysAlisPro, and datasets were prepared for subsequent structure solution and model building with PHENIX and COOT.

Figure 2. 1: Turkish DeLight Home Source XRD

Chapter 3:
RESULTS

3.1 Expression of EGFR-TKD

The recombinant expression of EGFR-TKD in *E. coli* Rosetta-II cells was successfully achieved in both mini-scale and large-scale cultures. Following induction with 0.4 mM IPTG, a distinct band at the expected molecular weight (~39 kDa with the SUMO tag and ~34 kDa after cleavage) was consistently detected on SDS-PAGE gels. Expression was evident under all induction conditions tested, including 16 °C overnight, 30 °C overnight, and 37 °C for 4 h. Despite these results, most of the expressed protein was localized in the insoluble pellet fraction, while only faint bands were observed in the soluble supernatant.

Mini-scale Ni-NTA pull-down assays further confirmed that the His-tagged EGFR-TKD was expressed efficiently but remained largely insoluble. Altering induction temperature did not significantly improve solubility. In contrast, the use of sarcosyl-containing lysis buffers (1.5% w/v) facilitated partial recovery of the protein in a soluble form. Urea treatment (2–8 M) was also able to solubilize the protein, but refolding attempts following denaturation resulted in unstable preparations with minimal retention of functional protein during subsequent purification steps.

In conclusion, EGFR-TKD was consistently overexpressed in *E. coli*; however, efficient recovery in soluble form required the use of detergent-assisted solubilization, with sarcosyl showing the most promising results among the tested strategies.

3.2 Expression of HER2-TKD

HER2-TKD was overexpressed in *E. coli* Rosetta-II cells harboring the pET28a(+) SUMO-tag construct. Induction with 0.4 mM IPTG at 37 °C resulted in detectable expression bands from the first hour post-induction, with increasing intensity up to 7 h. At longer induction times (8–16 h), additional lower molecular weight bands were observed, suggesting protein degradation. Based on SDS-PAGE analysis, 7 h at 37 °C was identified as the optimal induction period for HER2-TKD expression (Figure 3.1).

As observed with EGFR-TKD, HER2-TKD was predominantly localized to the insoluble fraction when cells were lysed using Triton X-100–based buffers. In contrast, lysis with 1.5% sarcosyl improved protein solubility, with clear bands appearing in the supernatant fraction. This confirmed that sarcosyl facilitated recovery of HER2-TKD in a soluble form suitable for downstream purification (Figure 3.2).

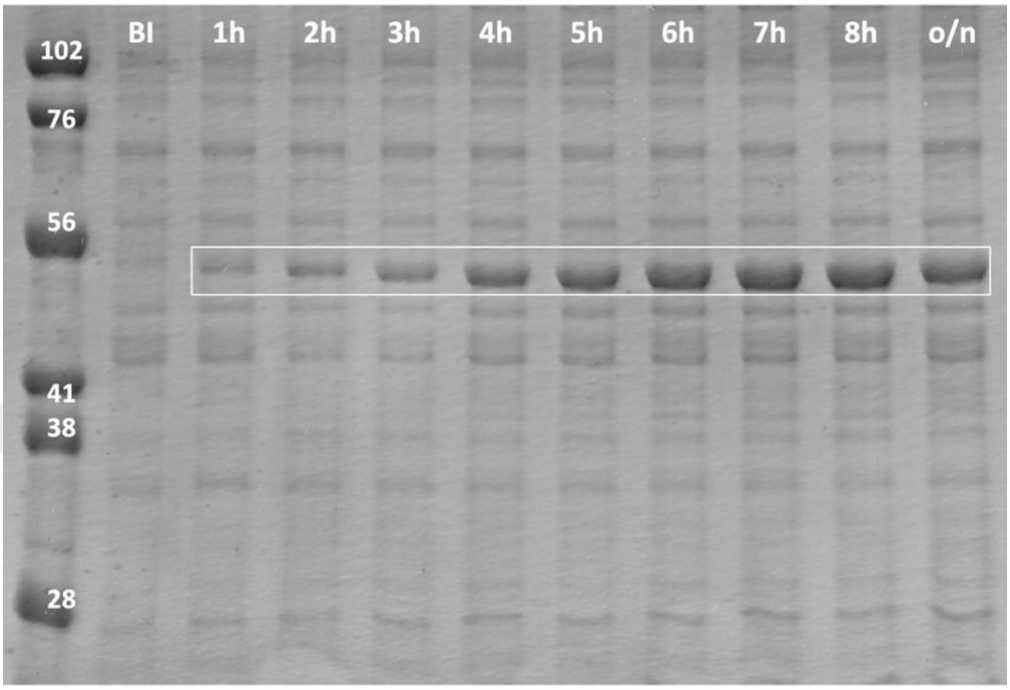

Figure 3. 1: SDS-PAGE analysis of HER2-TKD expression at different induction times. HER2-TKD expression was examined following induction with 0.4 mM IPTG at 37 °C. Whole-cell lysates (WCL) were collected at different time points post-induction (1–8 h and 16 h, overnight) and analyzed on a 12% SDS-PAGE gel. Lane 1: protein marker; Lane 2: before induction (BI); Lanes 3–11: samples collected at 1 h (Lane 3), 2 h (Lane 4), 3 h (Lane 5), 4 h (Lane 6), 5 h (Lane 7), 6 h (Lane 8), 7 h (Lane 9), 8 h (Lane 10), and 16 h (Lane 11, overnight). A distinct band at approximately 48 kDa, corresponding to HER2-TKD, increased in intensity up to 7 h post-induction. Beyond this time point, no further increase was observed. Based on these results, 7 h of induction was determined to be optimal for HER2-TKD expression. All lanes were loaded with 3 µL of sample.

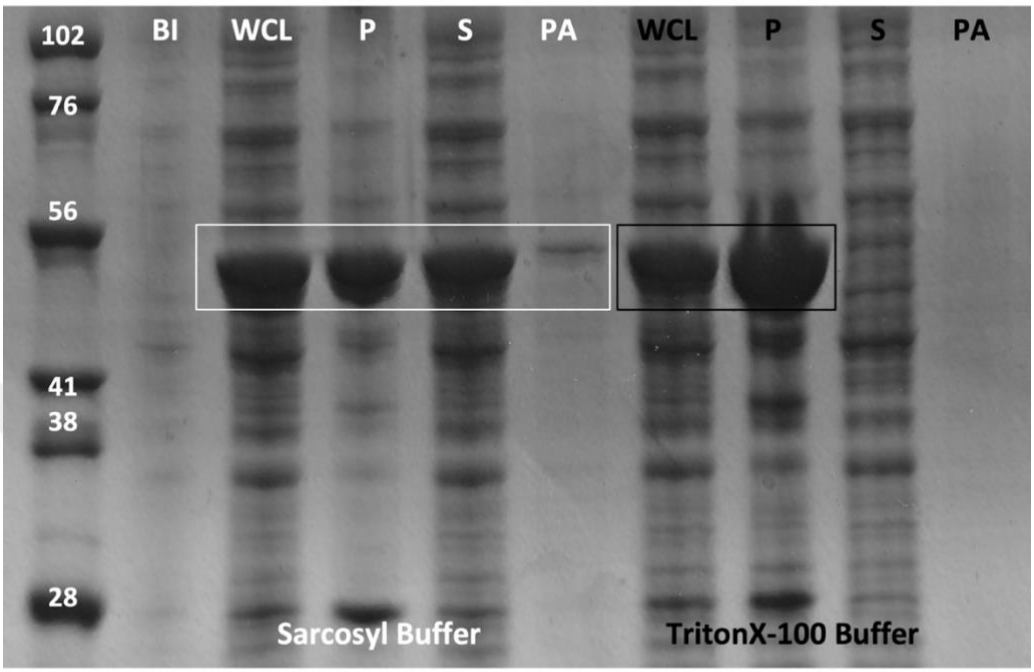

Figure 3. 2: Solubility analysis of HER2-TKD with and without Sarkosyl detergent by SDS-PAGE. HER2-TKD was expressed in *E. coli* Rosetta-II and induced with 0.4 mM IPTG at 37 °C for 7 h. After harvesting, cells were lysed using two different buffer systems: one containing 1.5% Sarkosyl (pH 8.5) and the other supplemented with Triton X-100 (no Sarkosyl). To evaluate the effect of detergents on protein solubility, whole-cell lysates (WCL), pellet (P), supernatant (S), and pull-down (PA) fractions were analyzed by 12% SDS-PAGE. Lane 1: protein marker; Lane 2: before induction (BI). Lanes 3–6: Sarkosyl-containing buffer (WCL, pellet, supernatant, pull-down). Lanes 7–10: Triton X-100 buffer (WCL, pellet, supernatant, pull-down). A band at ~48 kDa, corresponding to HER2-TKD, was mainly detected in the pellet fraction under Triton X-100 conditions, indicating poor solubility. In contrast, Sarkosyl-containing lysis resulted in increased recovery of HER2-TKD in the soluble fraction. Based on these results, subsequent purification steps were performed using Sarkosyl-based buffers. All lanes were loaded with 3 µL of sample.

3.3 Optimization of Induction and Solubilization

Systematic mini-scale experiments were conducted to evaluate the effects of induction conditions and lysis strategies.

IPTG concentration: For EGFR-TKD, induction trials were performed with IPTG concentrations ranging from 0.05 to 0.40 mM. While higher IPTG concentrations increased overall protein expression, they did not improve solubility. Based on these results, 0.4 mM IPTG was selected for subsequent experiments as it provided strong expression without apparent toxicity.

For HER2-TKD, IPTG concentration screening was not performed; instead, induction was carried out directly with 0.4 mM IPTG at 37 °C, which yielded reproducible expression and was therefore used in all downstream experiments.

Induction temperature and duration: EGFR-TKD expression was robust at 16 °C, 30 °C, and 37 °C; however, none of these conditions led to appreciable solubilization in non-sarcosyl buffers. The highest overall yield was achieved at 37 °C for 4 h, which was therefore used for scale-up. HER2-TKD showed a clear time-dependent profile, with maximum expression at ~7 h post-induction at 37 °C.

Detergent screening: Triton X-100 did not significantly improve solubility for either EGFR-TKD or HER2-TKD. In contrast, sarcosyl (1.5% w/v) consistently enabled partial solubilization in both proteins. This effect was reproducible across mini-scale and large-scale preparations.

Denaturant screening (urea): For EGFR-TKD, urea (0–8 M) enhanced solubilization but hampered downstream purification and refolding, limiting its utility. HER2-TKD was not extensively tested with urea, as sarcosyl proved sufficient for solubilization.

Host strain evaluation: EGFR-TKD was transformed into alternative strains (*E. coli* BL21 C43 and Gami-II). Colonies were obtained in C43 and Gami-II. Expression levels were comparable to Rosetta-II, and solubility did not improve, confirming Rosetta-II as a suitable production host.

Taken together, these optimizations established a reproducible strategy for both EGFR-TKD and HER2-TKD: induction at 37 °C (4 h for EGFR, 7 h for HER2) combined with sarcosyl-assisted lysis.

3.4 Purification Workflows and Tag Removal

After lysis and clarification, EGFR-TKD and HER2-TKD proteins were purified using Ni-NTA affinity chromatography. For EGFR-TKD, elution with 250 mM imidazole produced clear bands at the expected molecular weight, confirming successful recovery of the His_6-SUMO–tagged protein. In contrast, purification of HER2-TKD was less consistent, and partial protein loss was observed during binding and washing steps, which may be related to the use of detergent-containing buffers (Figure 3.3).

SUMO tag removal was carried out using ULP1 protease. For EGFR-TKD, cleavage conditions were systematically tested at different protease-to-substrate ratios, incubation temperatures, and time points (Figure 3.4). The most effective condition was obtained with a 5:1000 ratio of ULP1 at 4 °C, where efficient cleavage was achieved within 30 minutes (Figure 3.5). Reverse Ni-NTA affinity purification confirmed the successful separation of the tag-free EGFR-TKD in the flow-through, while His_6-tagged components—including uncleaved protein, cleaved SUMO fragment, and ULP1 protease—remained bound to the resin (Figure 3.6).

Final polishing was performed by size-exclusion chromatography (SEC). HER2-TKD elution resulted in two overlapping peaks, with SDS-PAGE analysis showing that fractions 9–13 contained the highest amount of target protein (Figure 3.7). EGFR-TKD, on the other hand, eluted predominantly as a monomeric species, with a smaller peak

corresponding to aggregates or higher-order forms (Figure 3.8). The purity of collected fractions was verified by SDS-PAGE (Figure 3.9).

Overall, EGFR-TKD purification yielded consistent results, with concentrated protein suitable for crystallization trials (approximately 2.0–2.4 mg/mL). HER2-TKD recovery was lower and less reproducible, underlining the greater challenge of obtaining this protein in high yield and purity compared to EGFR-TKD.

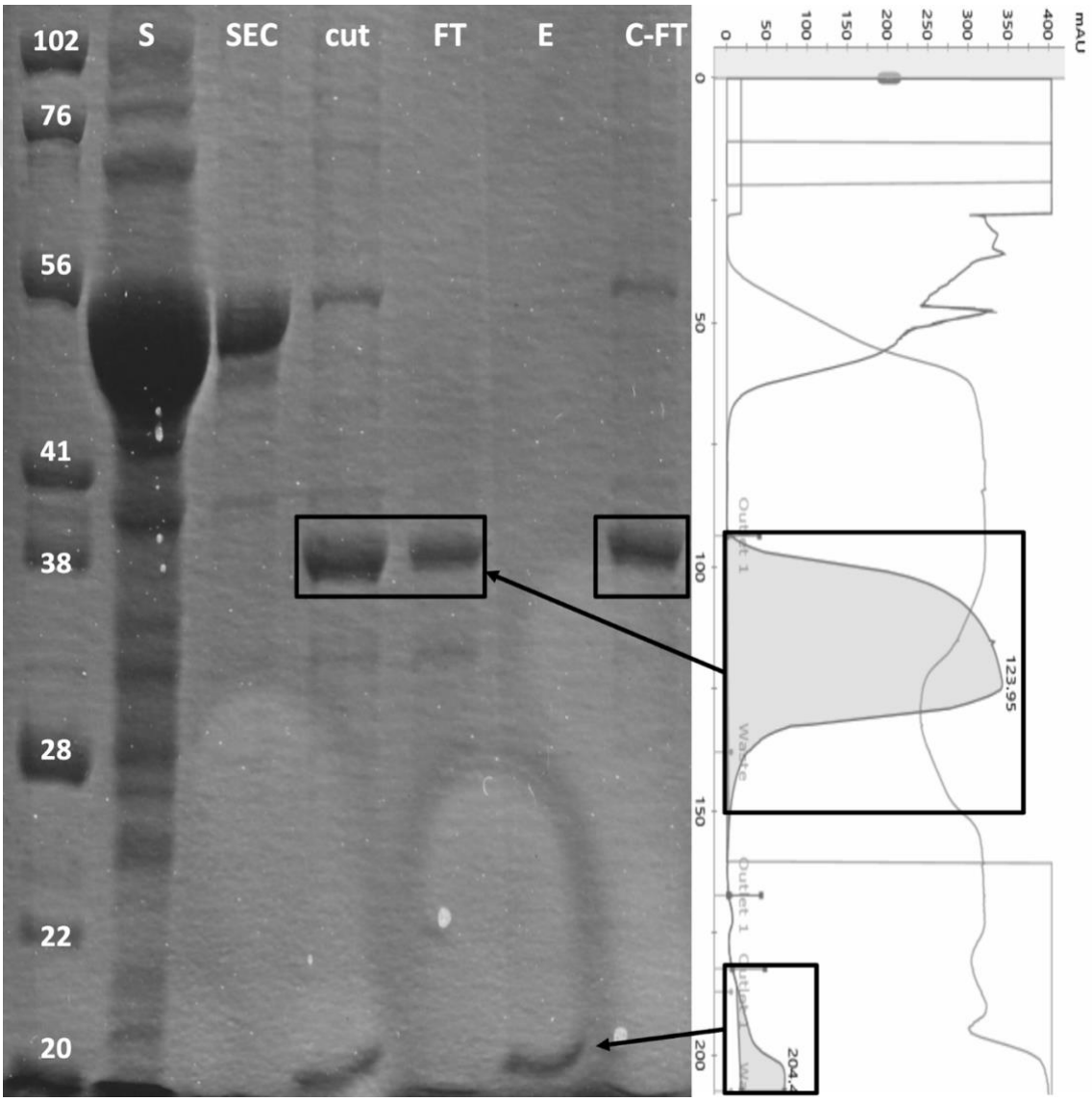

Figure 3. 3: Purification of HER2-TKD by reverse Ni-NTA affinity after His_6-SUMO tag cleavage. HER2-TKD (~48 kDa) was purified following His_6-SUMO tag (~35 kDa) removal by ULP1 protease. The efficiency of tag cleavage and subsequent purification was assessed by 12% SDS-PAGE. In the reverse Ni-NTA setup, untagged

HER2-TKD was recovered in the flow-through, while His_6-tagged species—including uncleaved fusion protein, the cleaved SUMO tag, and His-tagged ULP1 protease—were retained on the resin and later eluted.

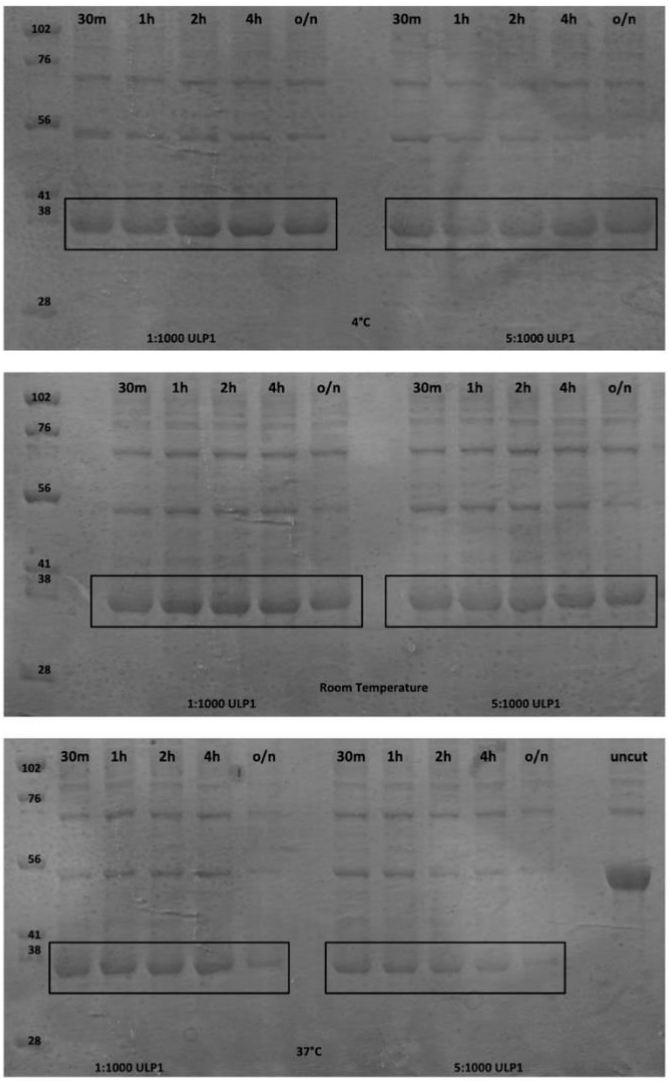

Figure 3. 4: Cleavage Test of SUMO-Tagged EGFR-TKD Using ULP1 at Different Ratios (1:1000 and 5:100), Temperatures (1st) 4°C, (2nd) Room Temperature, (3rd) 37°C, and Time Points (30 min, 1 h, 2 h, 4 h, and Overnight).

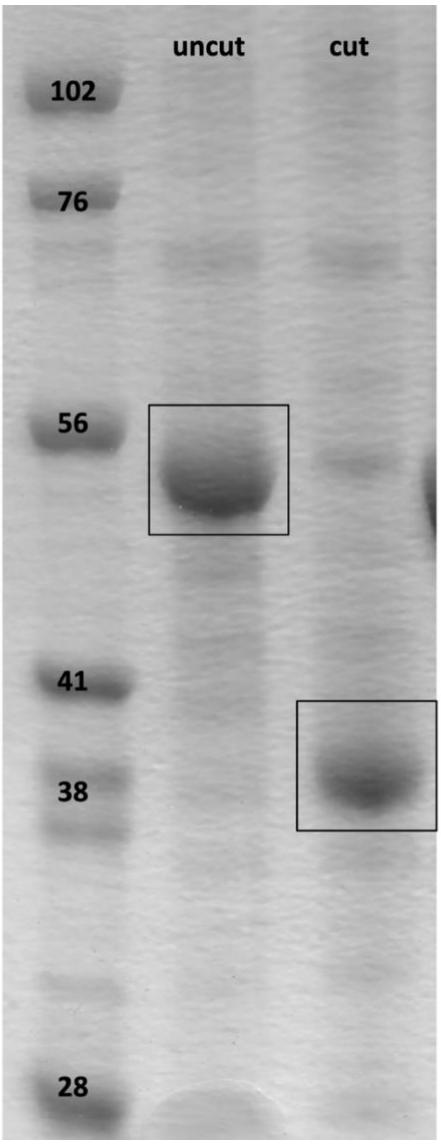

Figure 3. 5: 12% SDS-PAGE analysis of SUMO-tag cleavage of EGFR-TKD 5:1000 ULP1 at 4°C for 30 minutes.

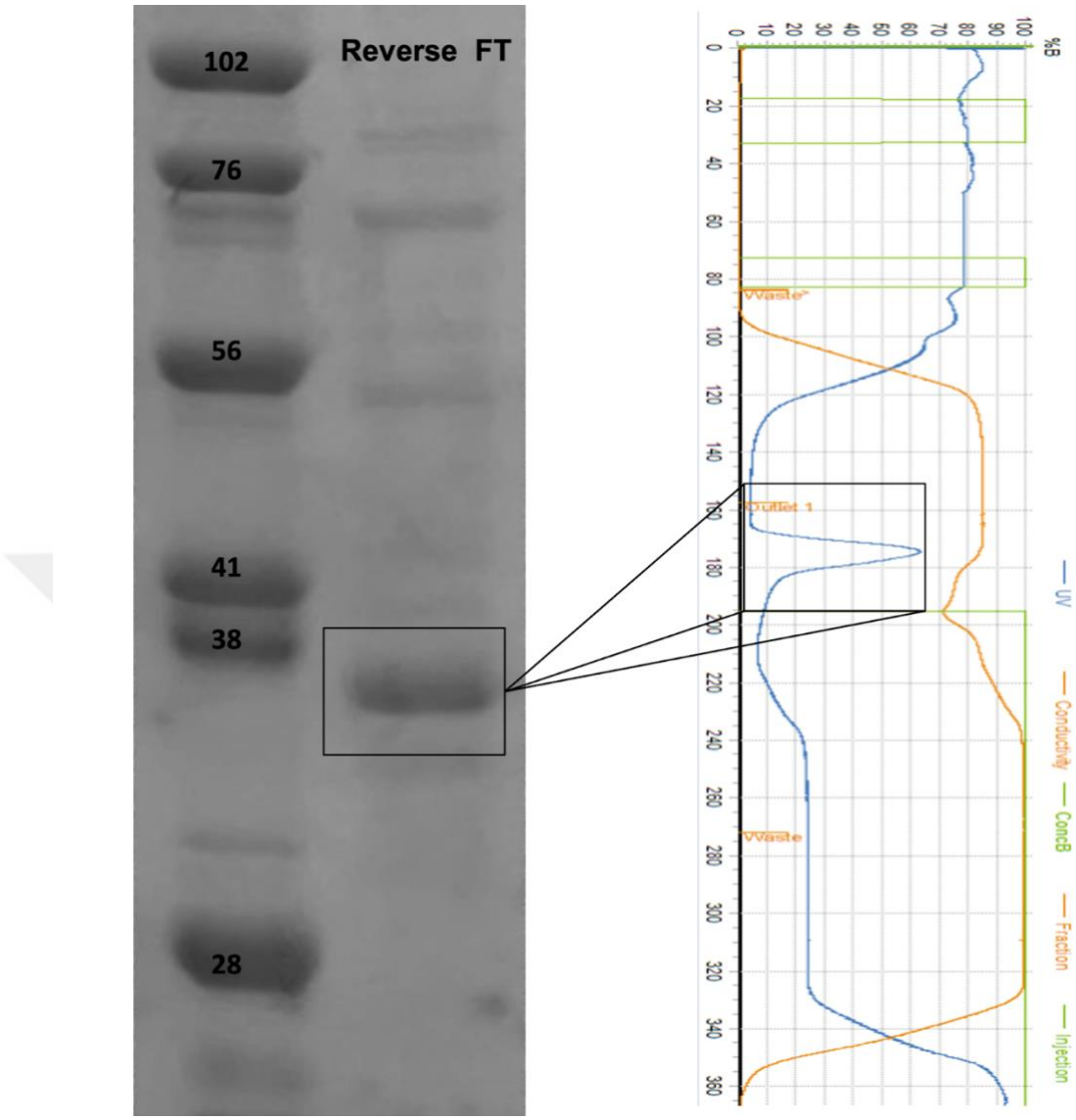

Figure 3. 6: EGFR-TKD tag removal via Ni-NTA affinity chromatography Graphical result and flow-throughs of the concentrated sample (2.4 mg/mL) analyzed on a 12% SDS gel.

Size-exclusion chromatography (Superdex 200) was employed for final polishing. EGFR-TKD eluted as a major peak with corresponding SDS-PAGE validation of purity. HER2-TKD elution showed two overlapping peaks, with the earlier fractions containing the majority of the target protein.

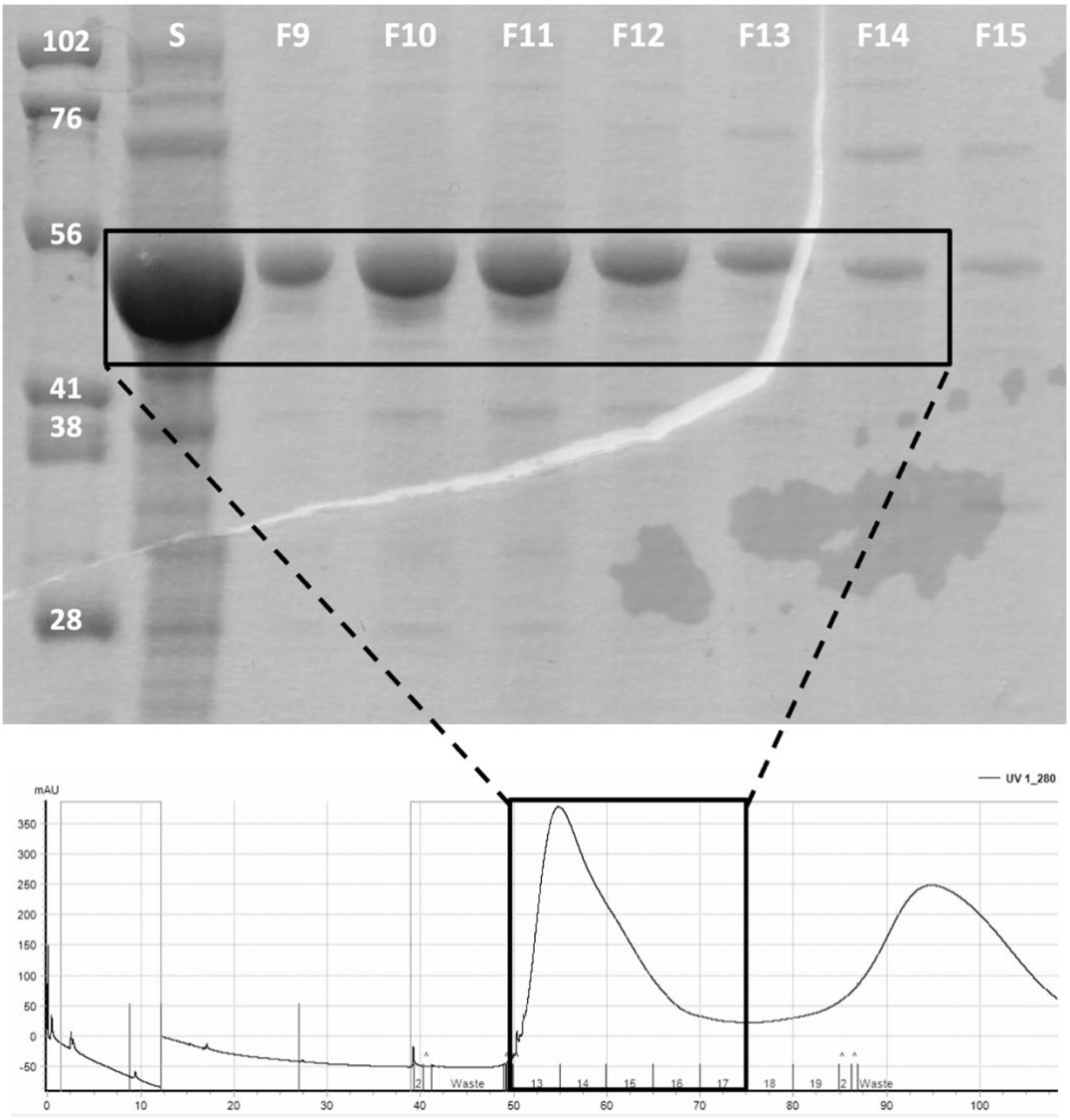

Figure 3. 7: Size-exclusion chromatography (SEC) purification of HER2-TKD and analysis of collected fractions by SDS-PAGE. HER2-TKD was purified by SEC using a Superdex-200 column. Fractions F9–F13 and F14–F21 were collected as indicated in the chromatogram. The collected fractions were analyzed by 12% SDS-PAGE. A distinct band at ~48 kDa, corresponding to HER2-TKD, was predominantly observed in fractions F9–F13, indicating that the target protein was enriched in this range.

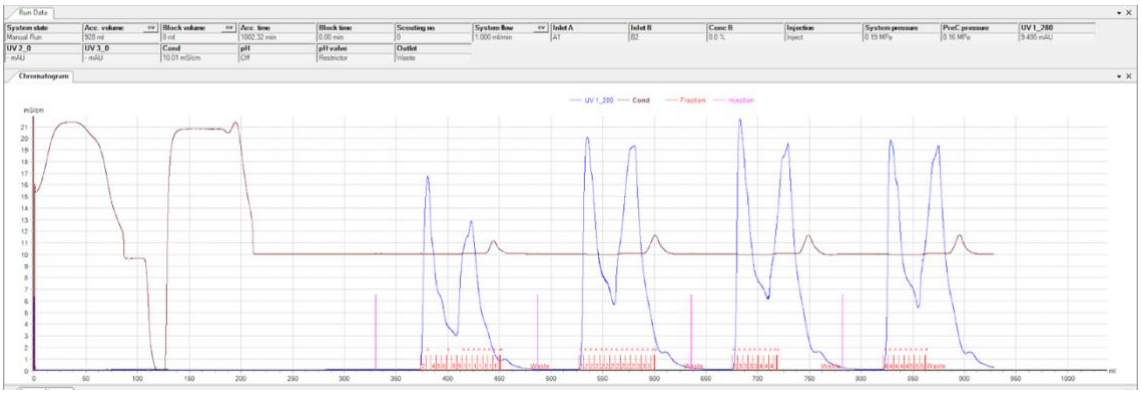

Figure 3. 8: Size-exclusion chromatography (SEC) profile of EGFR-TKD.

SEC analysis of EGFR-TKD showed two major peaks. The first, predominant peak corresponded to the monomeric form of the protein, while the later, smaller peak represented aggregated or higher-order species. The monomeric fractions were pooled and subsequently used for downstream structural studies and crystallization trials.

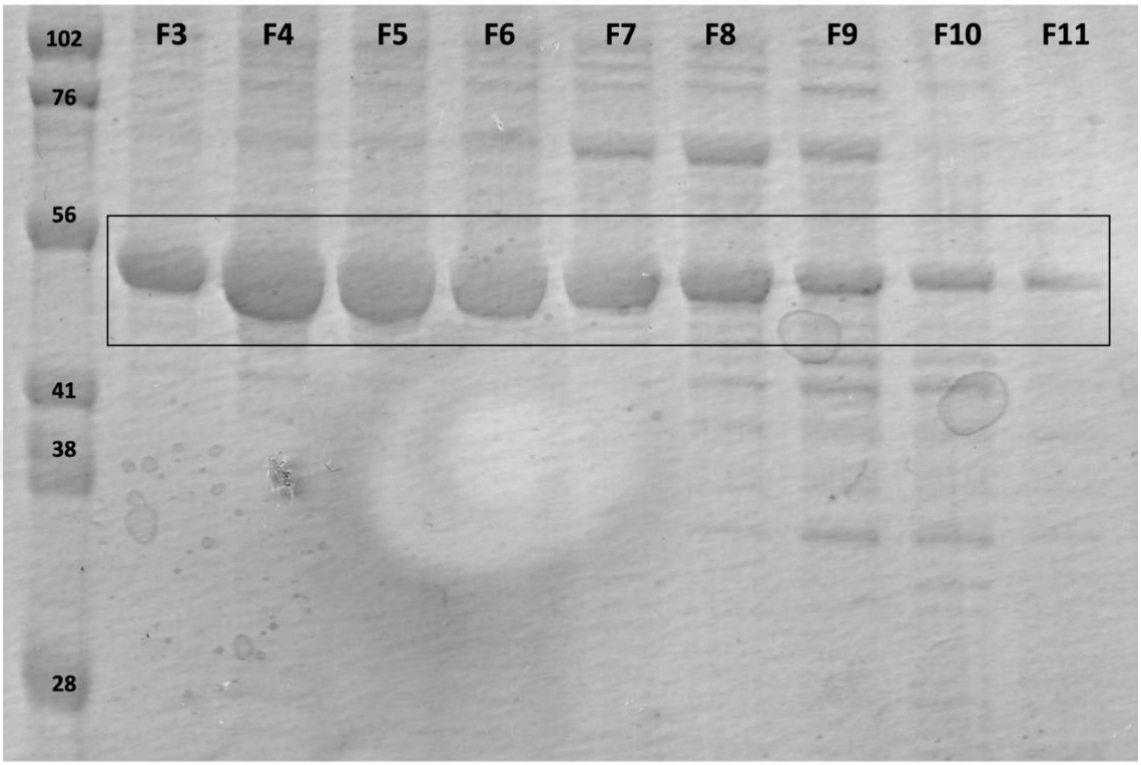

Figure 3. 9: 12% SDS-PAGE analysis of SEC fractions.

Protein yields varied across preparations. On average, EGFR-TKD preparations yielded ~2.0–2.4 mg/mL concentrated protein suitable for crystallization trials, whereas HER2-TKD recovery was lower and less consistent.

3.5 Crystallization Attempts and Observations

Crystallization experiments were carried out for both EGFR-TKD and HER2-TKD using the microbatch-under-oil method in Terasaki plates. A wide range of commercially available sparse-matrix screens were employed, corresponding to more than 3000 unique conditions. Trials were conducted in parallel at 4 °C and room temperature in order to evaluate the influence of temperature on crystal nucleation and growth.

The overall workflow of these trials, from protein preparation to crystallization setup and screening, is summarized in Figure 3.10. This workflow illustrates the systematic approach applied to both EGFR-TKD and HER2-TKD, starting with purified protein samples, followed by microbatch setup, and ending with microscopic inspection of drops for crystal formation.

Despite extensive screening, crystallization remained a major bottleneck, with most conditions yielding precipitate or amorphous aggregates rather than ordered crystals. Occasional microcrystalline material or weak diffraction-quality crystals were observed, particularly for EGFR-TKD in the presence of small-molecule inhibitors. These preliminary findings provided the basis for subsequent optimization experiments.

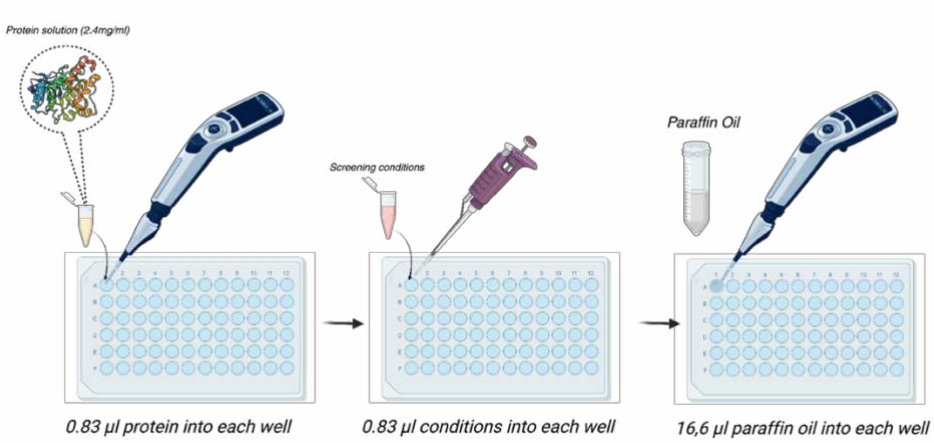

Figure 3. 10: Crystallization Workflow. Figure created with BioRender.

3.5.1 EGFR-TKD Crystallization Outcomes

Extensive crystallization trials were performed with purified EGFR-TKD using the microbatch-under-oil method in Terasaki plates. More than 3000 unique conditions were tested across multiple commercial screens, including Wizard, Crystal Screen, and Natrix formulations. Plates were incubated both at 4 °C and room temperature, and wells were inspected regularly over a four-week period.

In most conditions, EGFR-TKD yielded amorphous precipitates or microcrystalline aggregates. However, initial crystal formation was observed in specific conditions. Crystals were obtained in the NR-LBD-II screen (#42), containing 1.4 M lithium sulfate and 0.1 M Bis-Tris (pH 6.5). Additional crystalline material was detected under conditions with 0.25 M potassium thiocyanate and 27% PEG 3350 (pH 6.9). To improve crystal quality, drop ratio optimizations were carried out by varying reservoir volumes (0.70–1.25 µL) while maintaining 0.83 µL protein per drop.

Despite these optimization efforts, the resulting crystals remained small and poorly ordered, and no well-diffracting crystals were obtained. Representative microscopy images of these crystals, including apo and inhibitor-bound trials (e.g., erlotinib-bound EGFR-TKD), are shown in Figures 3.11 and 3.12. The chemical structure of the tested compound B-2 is presented in Figure 3.13. These results indicate that while EGFR-TKD could be produced in soluble form at preparative scale, its crystallization remains limited by intrinsic conformational flexibility and partial instability.

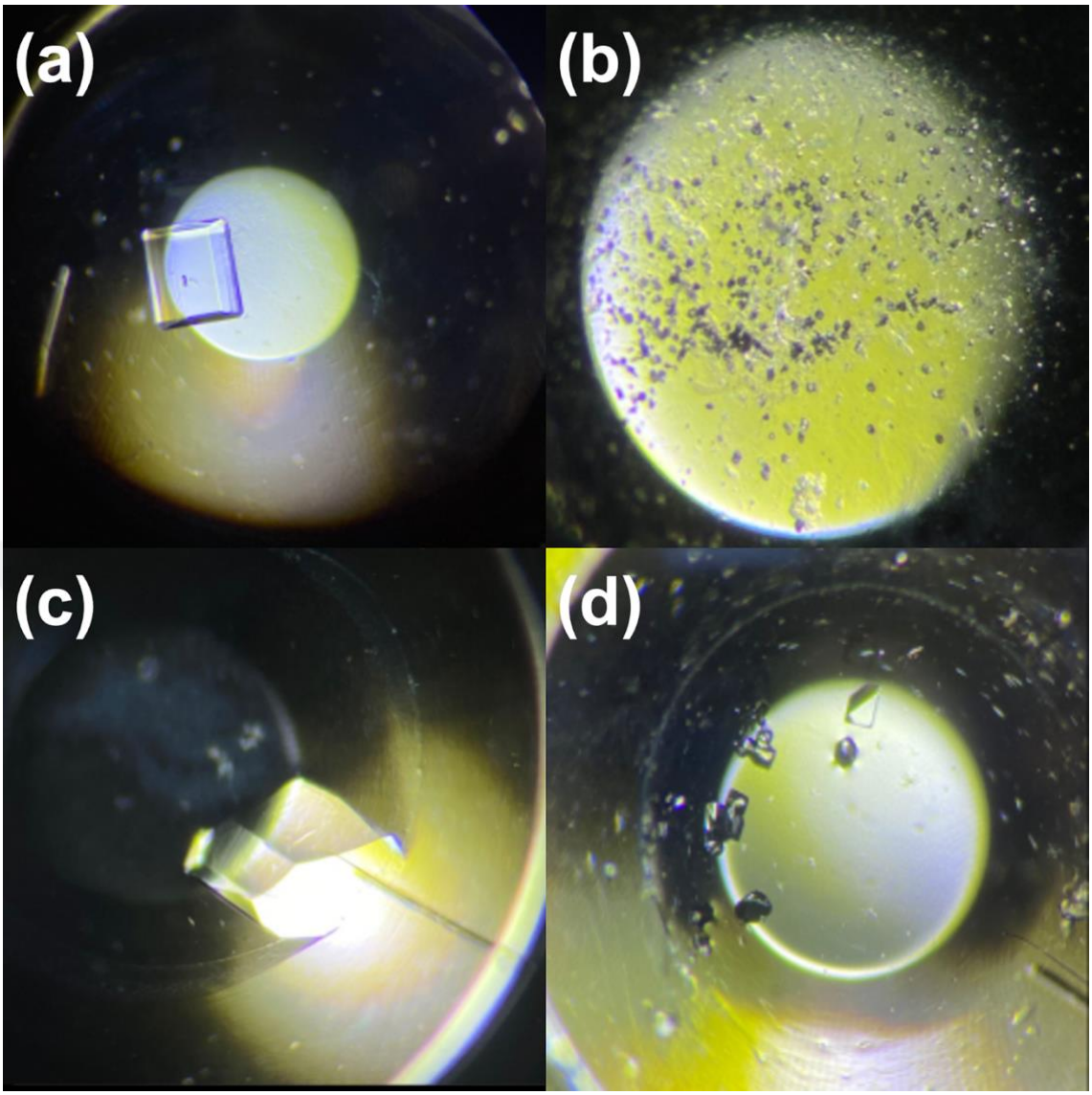

Figure 3. 11: Crystal photos (a) EGFR-TKD Crystal Cryo-II #29, (b) EGFR-TKD Index-II #16, (c) EGFR-TKD NR-LBD-II #42, (d) EGFR-TKD Grid/NaCl/No Malonate #18

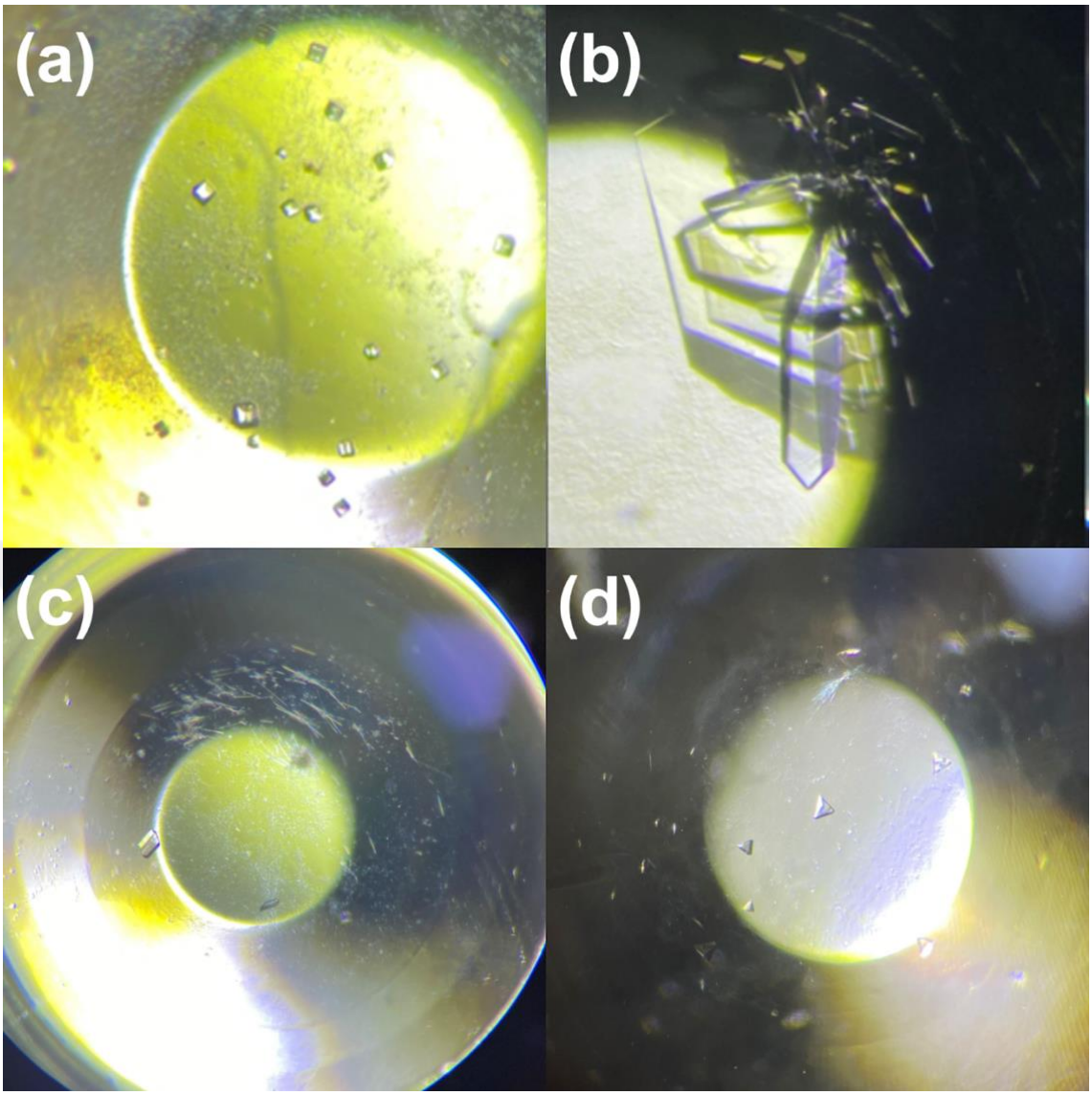

Figure 3. 12: Crystal photos (a) EGFR-TKD+Reference Drug Helix-I #22, (b) EGFR-TKD NR-LBD-II #41, (c) EGFR-TKD+Erlotinib Helix-I #32, (d) EGFR-TKD+Erlotinib Wizard

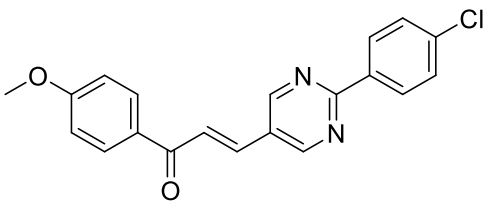

B-2

Figure 3. 13: The chemical structure of B-2.

3.5.2 HER2-TKD Crystallization Outcomes

Crystallization trials of HER2-TKD were conducted under both apo and inhibitor-bound conditions. Similar to EGFR-TKD, over 3000 sparse-matrix formulations were screened using the microbatch-under-oil method in Terasaki plates at 4 °C and room temperature. Initial observations revealed that HER2-TKD remained soluble under sarcosyl-assisted purification conditions, allowing for the setup of extensive crystallization experiments.

Co-crystallization with novel small-molecule inhibitors significantly improved crystal formation. Distinct morphologies were observed depending on the screening condition (Figure 3.14). Needle-like crystals were obtained in the NRLBD-I #33 screen, while Pact Premier II #22 produced well-defined crystals with improved size and shape. Block-shaped crystals were identified in the Wizard Synergy-II #1 formulation, and additional crystalline material was obtained from the Crystal Screen I #24 condition. Although these crystals showed varied morphologies, their presence confirmed that HER2-TKD can form ordered lattices when stabilized by inhibitor binding.

The chemical structures of the tested small-molecule compound B-2 used in co-crystallization assays are shown in Figure 3.13. These ligands were designed within our group as potential HER2/EGFR dual inhibitors and served as valuable tools for promoting crystal growth.

Together, these results demonstrate that HER2-TKD crystallization is more favorable under inhibitor-bound conditions compared to apo states, providing a promising starting point for future optimization and diffraction analysis.

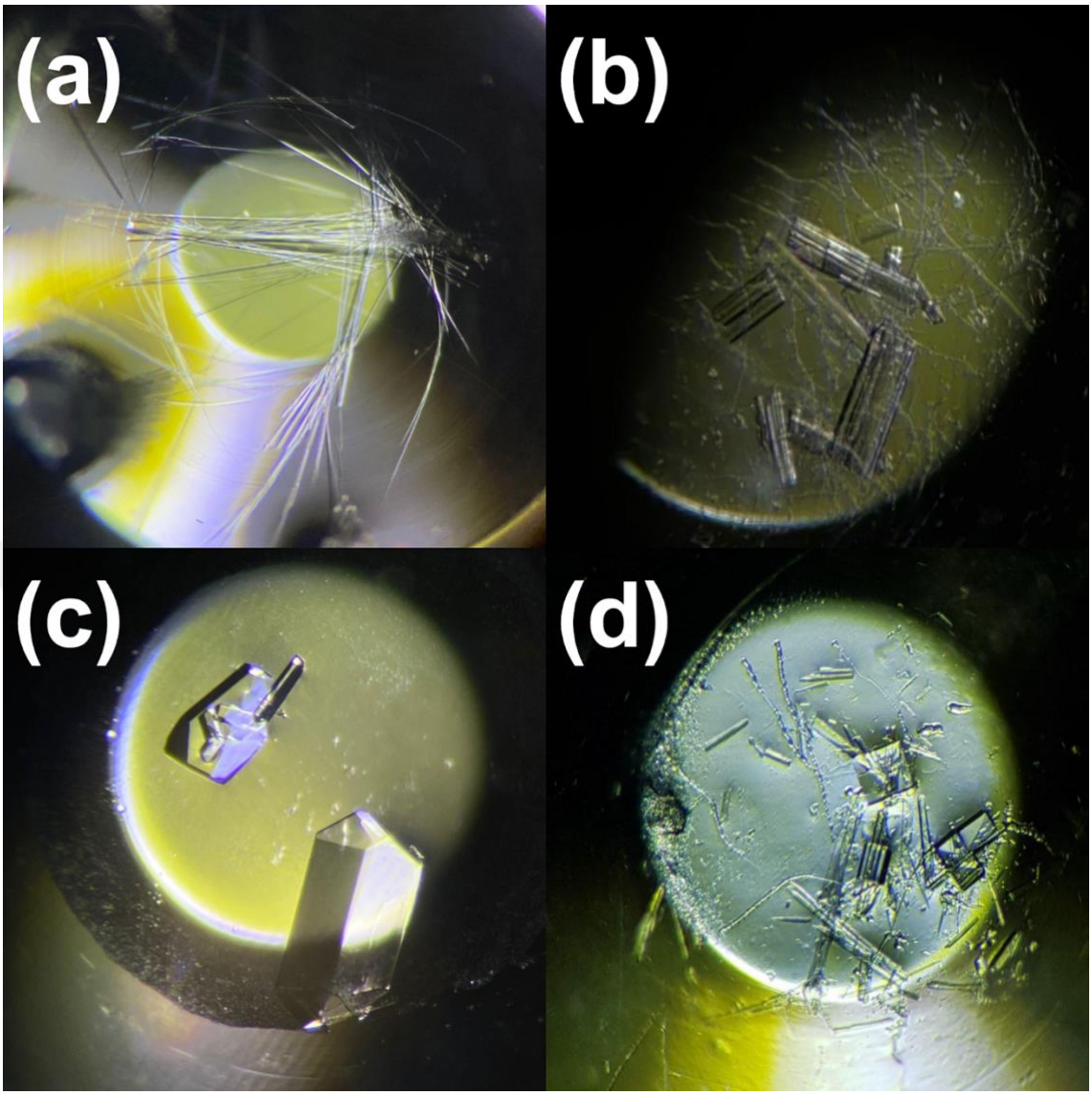

Figure 3. 14: The HER2-TKD crystals obtained through co-crystallization with novel inhibitors. Microscope images of HER2-TKD protein crystals formed after SUMO tag removal and protein concentration. Co-crystallization was carried out in the presence of novel small-molecule inhibitors. (a) Needle-like crystals formed in the NRLBD-I #33 condition. (b) Crystals obtained in the Pact Premier II #22 condition. (c) Block-shaped crystals formed in the Wizard Synergy-II #1 condition. (d) Crystals grown in Crystal Screen I #24 condition.

Chapter 4:
DISCUSSION AND CONCLUSION

4.1 Challenges in Recombinant Production of TKDs

The recombinant production of EGFR-TKD and HER2-TKD in *E. coli* presented several difficulties, most of which are well-documented for receptor tyrosine kinases. In both cases, the proteins were expressed at high levels, but the majority of the product was recovered in the insoluble pellet fraction. This outcome is in line with the tendency of RTKs to misfold and aggregate when expressed in prokaryotic hosts, largely due to their hydrophobic patches, conformational complexity, and reliance on eukaryotic folding machinery.

Detergent-assisted solubilization was tested as a strategy to overcome these limitations. Sarcosyl, in particular, was effective in releasing a portion of the protein into the soluble fraction for both EGFR and HER2. However, its use also introduced a major drawback: the detergent interfered with His-tag binding to Ni-NTA resin, leading to reduced recovery during affinity purification. This observation is consistent with earlier reports and emphasizes a recurring challenge in the bacterial production of TKDs: methods that increase solubility often compromise the efficiency of downstream purification.

In this study, several alternative strategies were explored to address this issue. Tag removal followed by reverse Ni-NTA purification, together with additional steps such as size-exclusion chromatography, was found to provide partial improvements in protein quality and recovery. These approaches proved particularly useful for separating detergent-sensitive proteins from uncleaved or aggregated species. However, the overall yields remained modest, highlighting the intrinsic difficulty of producing stable and properly folded TKDs in bacterial systems.

4.2 Comparison of EGFR and HER2 TKD Workflows

Although EGFR-TKD and HER2-TKD were processed with the same expression and purification strategy, they behaved in strikingly different ways. EGFR-TKD was reliably produced across all induction conditions, yet most of it consistently ended up in the insoluble fraction, leaving only a small portion in the soluble state when detergents were not used. The addition of sarcosyl improved solubilization, but successful purification still relied on further interventions such as tag removal and reverse Ni-NTA chromatography. This pattern echoed what has been seen before, where detergents often enable recovery but complicate downstream purification.

HER2-TKD, on the other hand, followed a very different trajectory. Its expression reached a peak roughly seven hours after IPTG induction at 37 °C, but soon after, degradation bands became increasingly visible, reflecting its reduced stability compared with EGFR-TKD. This instability aligned well with the idea that HER2-TKD is more conformationally flexible and vulnerable to proteolysis. Sarcosyl again helped with solubilization, but downstream processing remained difficult: even after dialysis, a portion of HER2-TKD could not bind efficiently to Ni-NTA resin, leading to lower yields.

Together, these findings show that even proteins belonging to the same receptor family can present distinct challenges. EGFR-TKD proved relatively stable in expression but required aggressive solubilization to be useful, while HER2-TKD needed careful timing and more refined purification conditions. The contrast between them illustrates how each protein's unique biochemistry demands its own optimization, a reminder that success in structural biology often depends on adapting the workflow to the specific target at hand.

4.3 Crystallization Challenges and Structural Insights

Crystallization trials of EGFR-TKD and HER2-TKD involved broad screening across thousands of commercial conditions, both at low and ambient temperatures. In the case of EGFR-TKD, small crystal-like structures first appeared under NR-LBD-II conditions (1.4 M lithium sulfate, 0.1 M Bis-Tris, pH 6.5). Adjusting drop ratios yielded slightly more defined material, yet none of the crystals diffracted to useful resolution. Additional tests with PEG-based precipitants or salts such as potassium thiocyanate resulted in microcrystalline aggregates, again without sufficient diffraction.

For HER2-TKD, crystalline material was also observed, but diffraction analysis showed that many of these were salt crystals, a frequent complication of high-precipitant sparse-matrix screens. Needle-like and block-shaped crystals occasionally appeared, but none were verified as proteinaceous.

These findings are in line with earlier reports, emphasizing the challenges of crystallizing isolated tyrosine kinase domains (Stamos et al., 2002; Yun et al., 2007; Aertgeerts et al., 2011). Both EGFR and HER2 TKDs exhibit high conformational flexibility, and the absence of stabilizing regions contributes to structural heterogeneity. While soluble protein was obtained, crystallization remained a bottleneck, suggesting that future efforts may benefit from co-crystallization with inhibitors, detergent-assisted screening, or microseeding.

The lack of well-diffracting crystals in this study can be explained by both intrinsic properties of the proteins and experimental limitations. EGFR-TKD and HER2-TKD are highly flexible enzymes, particularly around the activation loop and C-terminal regions. This flexibility allows them to adopt multiple conformations in solution, which makes it difficult for them to form a uniform and well-ordered crystal lattice. Without a stabilizing ligand or mutation that locks the kinase into a single conformation, the protein population likely remained heterogeneous, resulting in poorly ordered or non-diffracting crystals.

Another contributing factor could be the presence of detergents used during solubilization. Even small amounts of residual sarcosyl or Triton X-100 may have interfered with crystal packing by masking hydrophobic surface patches or altering intermolecular interactions essential for lattice formation. Furthermore, expressing these kinases in *E. coli* may have introduced folding variations or lacked post-translational modifications, both of which can negatively affect crystal quality. Finally, since most conditions tested were based on commercial sparse-matrix screens, they may not have captured the delicate balance of precipitant concentration, pH, and temperature required for nucleation.

Considering these factors, the absence of good-quality crystals is consistent with the behavior of other receptor tyrosine kinases reported in the literature. Future crystallization attempts could benefit from using ligand-bound forms, stabilizing mutations, or microseeding techniques to promote the formation of more ordered and diffracting crystals.

4.4 Relevance to Structure-Based Drug Discovery

Although crystallization of EGFR-TKD and HER2-TKD remains a considerable bottleneck, the successful production of soluble protein in bacterial systems represents an important milestone for structure-guided drug discovery. Recombinant TKDs provide the biochemical foundation required for co-crystallization experiments, inhibitor binding assays, and mechanistic studies that can ultimately accelerate the rational design of novel therapeutic agents.

In the context of structure-guided drug discovery, understanding the molecular basis of tyrosine kinase inhibition is essential. Table 1.1 summarizes the FDA-approved small-molecule EGFR tyrosine kinase inhibitors (TKIs), classified by generation and inhibition mechanism (Topalan et al., 2025). These inhibitors illustrate how successive generations of TKIs have been developed to overcome resistance mutations such as T790M and C797S, progressing from reversible ATP-competitive inhibitors to irreversible covalent binders with higher selectivity for mutant EGFR. The mechanistic transition between

generations also reflects the structural adaptability of the EGFR kinase domain, which can shift between active and inactive conformations depending on ligand occupancy and mutation state.

This progressive evolution provides a structural framework for comparison with the novel inhibitors currently being developed within our research group. Building on these principles, our team designed and synthesized pyrazoline–thiazole hybrid scaffolds as potential next-generation EGFR inhibitors (Sever et al., 2025). Prior studies demonstrated that Compound I exerted a marked anti-NSCLC effect, with an IC_{50} of 10.76 μM, surpassing the clinical reference erlotinib (22.35 μM). In enzymatic assays, the same compound inhibited EGFR with an IC_{50} of 4.34 μM (Sever et al., 2019). Similarly, Compound II, containing a naphthyl substitution, showed improved potency relative to lapatinib, with an anti-NSCLC IC_{50} of 9.51 μM versus 16.44 μM for the reference drug, and 58.32% EGFR inhibition at 10 μM (Çiftçi et al., 2024). More recently, the B-4 scaffold exhibited notable anti-NSCLC activity (IC_{50} = 20.49 ± 2.71 μM) alongside 46% EGFR inhibition at 10 μM (Reymova et al., 2025).

The recombinant production of soluble EGFR-TKD achieved in this study establishes the experimental foundation for future co-crystallization and binding assays with these newly developed scaffolds. Structural characterization of these complexes will not only validate the proposed binding models but also guide the rational design of compounds with improved selectivity, potency, and resistance profiles.

Parallel efforts targeting HER2 are of equal importance, given the increasing clinical relevance of HER2 alterations in NSCLC and other malignancies. The ability to recover HER2-TKD in a soluble state, even with detergent-assisted protocols, provides a critical experimental basis for downstream applications. Co-crystallization with HER2-selective inhibitors or antibody fragments could support the structural characterization of HER2 variants that remain poorly understood compared with EGFR.

Taken together, these results demonstrate that although crystallization hurdles persist, the workflows established in this thesis directly contribute to structure-based drug discovery. By combining soluble TKD production with inhibitor design and preclinical

evaluation, future studies will be well positioned to deliver candidate molecules with improved selectivity, potency, and resistance profiles against EGFR- and HER2-driven NSCLC.

4.5 Future Directions

The findings of this study highlight several avenues for future research. A primary limitation of the present work was the reliance on bacterial expression systems, which, although efficient and cost-effective, do not replicate eukaryotic post-translational modifications. Moving forward, expression of EGFR-TKD and HER2-TKD in eukaryotic hosts such as insect (Sf9) or mammalian cells could provide more physiologically relevant protein preparations with improved folding and solubility (Seifert et al., 2016). Such systems may also reduce the tendency for aggregation and improve crystallization outcomes.

In terms of purification, strategies that bypass detergent interference warrant further exploration. Reverse Ni-NTA following SUMO-tag cleavage, or workflows prioritizing size-exclusion chromatography before affinity purification, may help reduce sample loss and improve homogeneity. Co-expression with molecular chaperones or the application of refolding protocols optimized for tyrosine kinases could also enhance the recovery of properly folded protein (Bukowska & Grütter, 2013).

Crystallization remains a critical challenge. The results presented here suggest that the intrinsic flexibility of isolated kinase domains hampers lattice formation. Future studies could revisit crystallization using ligand-bound complexes, which are known to stabilize specific conformations of RTKs (Yun et al., 2007). In addition, rational mutagenesis approaches such as surface entropy reduction may promote the formation of well-ordered crystals, while advanced methods including additive screening or microseeding could further increase success rates (Derewenda, 2010).

Finally, while X-ray crystallography has been the primary tool for structure determination, complementary biophysical methods should also be considered. Cryo-electron microscopy (cryo-EM) now enables visualization of protein complexes at near-atomic resolution without the need for crystals, making it a promising avenue for future studies of ErbB receptors. Similarly, hydrogen–deuterium exchange mass spectrometry (HDX-MS) could provide valuable insights into the conformational dynamics of EGFR and HER2, complementing structural snapshots obtained by crystallography or cryo-EM.

By building upon the expression and solubilization strategies established in this thesis, future work can move closer to achieving high-resolution structural characterization of EGFR and HER2 TKDs. These efforts will not only expand our fundamental understanding of ErbB receptor biology but also provide a structural framework for the rational design of next-generation inhibitors targeting resistant variants in NSCLC and related cancers.

4.6 Limitations of the Study

While this work establishes important groundwork for the recombinant production and preliminary crystallization of EGFR-TKD and HER2-TKD, several limitations must be acknowledged.

First, all protein expression was performed in E. coli. Although bacterial systems are cost-effective and allow rapid production, they do not provide eukaryotic post-translational modifications such as glycosylation or phosphorylation, which are known to influence receptor tyrosine kinase folding, stability, and function (Yarden & Pines, 2012). The absence of these modifications may partly explain the tendency of both TKDs to accumulate in inclusion bodies and the challenges encountered during crystallization.

Second, recovery of soluble protein relied heavily on detergent-assisted solubilization. In particular, sarcosyl proved effective in disrupting inclusion bodies; however, its presence interfered with standard affinity purification, likely by masking or destabilizing the His-tag binding site. Although dialysis and reverse Ni-NTA strategies

partially alleviated this problem, it remains uncertain whether residual detergent influenced crystallization competency, as detergents are known to destabilize some protein–protein or protein–ligand interactions during lattice formation (Holcomb et al., 2017).

Third, crystallization trials were primarily restricted to commercially available sparse-matrix screens. While these formulations provide a broad initial survey, they may not capture the more tailored conditions often required for kinases, particularly those with flexible activation loops or unstable regulatory regions (McPherson & Gavira, 2014). Alternative approaches such as additive screens, microseeding, or co-crystallization with stabilizing ligands were only tested in a limited fashion and could provide more favorable outcomes in future work.

Finally, although milligram quantities of protein were obtained, the yields were not sufficiently consistent to sustain repeated crystallization campaigns, especially for HER2-TKD. This limited the ability to perform extensive optimization or replicate promising conditions. Variability in yield and solubility remains a practical constraint that will need to be addressed before large-scale structural studies can be routinely pursued.

BIBLIOGRAPHY

Aertgeerts, K., Skene, R., Yano, J., Sang, B. C., Zou, H., Snell, G., Jennings, A., Iwamoto, K., Habuka, N., Hirokawa, A., Ishikawa, T., Tanaka, T., Miki, H., Ohta, Y., & Sogabe, S. (2011). Structural analysis of the mechanism of inhibition and allosteric activation of the kinase domain of HER2 protein. Journal of Biological Chemistry, 286(21), 18756–18765. https://doi.org/10.1074/jbc.M110.190165

Chayen, N. E., & Saridakis, E. (2008). Protein crystallization: From purified protein to diffraction-quality crystal. Nature Methods, 5(2), 147–153. https://doi.org/10.1038/nmeth.f.202

Çiftçi, H., Otsuka, M., Fujita, M., & Sever, B. (2024). New naphthalene-linked pyrazoline–thiazole hybrids as prominent antilung and anti-breast cancer inhibitors. Turkish Journal of Chemistry, 48(6), 856–866. https://doi.org/10.55730/1300-0527.3704

Falls, D. (2003). Neuregulins: Functions, forms, and signaling strategies. Experimental Cell Research, 284(1), 14–30. https://doi.org/10.1016/s0014-4827(02)00102-7

Ferguson, K. M., Berger, M. B., Mendrola, J. M., Cho, H. S., Leahy, D. J., & Lemmon, M. A. (2003). EGF activates its receptor by removing interactions that autoinhibit ectodomain dimerization. Molecular Cell, 11(2), 507–517. https://doi.org/10.1016/s1097-2765(03)00047-9

Frezzetti, D., Caridi, V., Marra, L., et al. (2024). The impact of inadequate exposure to epidermal growth factor receptor-tyrosine kinase inhibitors on the development of

resistance in non-small-cell lung cancer cells. International Journal of Molecular Sciences, 25(9), 4844. https://doi.org/10.3390/ijms25094844

Giegé, R., Ducruix, A., & Timmins, P. (1995). Protein crystallization: Techniques, strategies, and tips. Acta Crystallographica Section D: Biological Crystallography, 51(2), 115–126. https://doi.org/10.1107/S0907444994011573

Harris, R. (2003). EGF receptor ligands. Experimental Cell Research, 284(1), 2–13. https://doi.org/10.1016/s0014-4827(02)00105-2

Holcomb, J., Spellmon, N., Zhang, Y., Dougherty, S., & Li, C. (2017). Protein crystallization: Eluding the bottleneck of X-ray crystallography. AIMS Biophysics, 4(4), 557–575. https://doi.org/10.3934/biophy.2017.4.557

Hubbard, S. R. (1999). Structural analysis of receptor tyrosine kinases. Progress in Biophysics and Molecular Biology, 71(3–4), 343–358. https://doi.org/10.1016/s0079-6107(98)00047-9

Hubbard, S. R. (2004). Juxtamembrane autoinhibition in receptor tyrosine kinases. Nature Reviews Molecular Cell Biology, 5(6), 464–471. https://doi.org/10.1038/nrm1399

Janmaat, M. L., Kruyt, F. A., Rodriguez, J. A., & Giaccone, G. (2003). Response to epidermal growth factor receptor inhibitors in non-small cell lung cancer cells: Limited antiproliferative effects and absence of apoptosis associated with persistent activity of extracellular signal-regulated kinase or Akt kinase pathways. Clinical Cancer Research, 9(6), 2316–2326.

Johnson, M., Garassino, M. C., Mok, T., & Mitsudomi, T. (2022). Treatment strategies and outcomes for patients with EGFR-mutant non-small cell lung cancer resistant to EGFR tyrosine kinase inhibitors: Focus on novel therapies. Lung Cancer, 170, 41–51. https://doi.org/10.1016/j.lungcan.2022.05.011

Jura, N., Endres, N. F., Engel, K., et al. (2009). Mechanism for activation of the EGF receptor catalytic domain by the juxtamembrane segment. Cell, 137(7), 1293–1307. https://doi.org/10.1016/j.cell.2009.04.025

Lemmon, M. A., & Schlessinger, J. (2010). Cell signaling by receptor tyrosine kinases. Cell, 141(7), 1117–1134. https://doi.org/10.1016/j.cell.2010.06.011

Lemmon, M. A., Schlessinger, J., & Ferguson, K. M. (2014). The EGFR family: Not so prototypical receptor tyrosine kinases. Cold Spring Harbor Perspectives in Biology, 6(4), a020768. https://doi.org/10.1101/cshperspect.a020768

Lenferink, A. E. G. (1998). Differential endocytic routing of homo- and hetero-dimeric ErbB tyrosine kinases confers signaling superiority to receptor heterodimers. EMBO Journal, 17(12), 3385–3397. https://doi.org/10.1093/emboj/17.12.3385

Levantini, E., Maroni, G., Del Re, M., & Tenen, D. G. (2022). EGFR signaling pathway as therapeutic target in human cancers. Seminars in Cancer Biology, 85, 253–275. https://doi.org/10.1016/j.semcancer.2022.04.002

McPherson, A., & Gavira, J. A. (2014). Introduction to protein crystallization. Acta Crystallographica Section F: Structural Biology Communications, 70(1), 2–20. https://doi.org/10.1107/S2053230X13033141

Mishra, S., Mutt, E., & Kar, R. K. (2012). Protein crystallography: Methods and protocols. International Journal of Bioscience, Biochemistry and Bioinformatics, 2(6), 414–423. https://doi.org/10.7763/IJBBB.2012.V2.123

Moasser, M. M. (2007). The oncogene HER2: Its signaling and transforming functions and its role in human cancer pathogenesis. Oncogene, 26(45), 6469–6487. https://doi.org/10.1038/sj.onc.1210477

Morrow, M. R., & Grant, C. W. M. (2000). The EGF receptor transmembrane domain: Peptide–peptide interactions in fluid bilayer membranes. Biophysical Journal, 79(4), 2024–2032. https://doi.org/10.1016/S0006-3495(00)76450-2

Ogiso, H., Ishitani, R., Nureki, O., et al. (2002). Crystal structure of the complex of human epidermal growth factor and receptor extracellular domains. Cell, 110(6), 775–787. https://doi.org/10.1016/s0092-8674(02)00963-7

Olayioye, M. A. (2000). The ErbB signaling network: Receptor heterodimerization in development and cancer. EMBO Journal, 19(13), 3159–3167. https://doi.org/10.1093/emboj/19.13.3159

Oxnard, G. R., Lo, P. C., Nishino, M., et al. (2013). Natural history and molecular characteristics of lung cancers harboring EGFR exon 20 insertions. Journal of Thoracic Oncology, 8(2), 179–184. https://doi.org/10.1097/JTO.0b013e3182779d18

Pao, W., & Chmielecki, J. (2010). Rational, biologically based treatment of EGFR-mutant non–small-cell lung cancer. Nature Reviews Cancer, 10(11), 760–774. https://doi.org/10.1038/nrc2947

Reymova, F., Sever, B., Topalan, E., et al. (2025). Design, synthesis, and mechanistic anticancer evaluation of new pyrimidine-tethered compounds. Pharmaceuticals, 18(2), 270. https://doi.org/10.3390/ph18020270

Riudavets, M., Sullivan, I., Abdayem, P., & Planchard, D. (2021). Targeting HER2 in non-small-cell lung cancer (NSCLC): A glimpse of hope? An updated review on therapeutic strategies in NSCLC harbouring HER2 alterations. ESMO Open, 6(5), 100260. https://doi.org/10.1016/j.esmoop.2021.100260

Roskoski, R., Jr. (2014). The ErbB/HER family of protein-tyrosine kinases and cancer. Pharmacological Research, 79, 34–74. https://doi.org/10.1016/j.phrs.2013.11.002

Sever, B., Altıntop, M. D., Radwan, M. O., et al. (2019). Design, synthesis and biological evaluation of a new series of thiazolyl-pyrazolines as dual EGFR and HER2 inhibitors. European Journal of Medicinal Chemistry, 182, 111648. https://doi.org/10.1016/j.ejmech.2019.111648

Sever B, Otsuka M, Fujita M, Ciftci H. Design, Synthesis, and Anticancer Evaluation of New Small-Molecule EGFR Inhibitors Targeting NSCLC and Breast Cancer. Int J Mol Sci. 2025 Jul 22;26(15):7065. doi: 10.3390/ijms26157065

Shi, F., Telesco, S. E., Liu, Y., Radhakrishnan, R., & Lemmon, M. A. (2010). ErbB3/HER3 intracellular domain is competent to bind ATP and catalyze autophosphorylation. Proceedings of the National Academy of Sciences, 107(17), 7692–7697. https://doi.org/10.1073/pnas.1002753107

Smyth, D. R., & Martin, J. L. (2000). X-ray crystallography: Structure determination of biological macromolecules. Biochemical and Molecular Biology Education, 28(1), 12–20. https://doi.org/10.1111/j.1539-3429.2000.tb00006.x

Stamos, J., Sliwkowski, M. X., & Eigenbrot, C. (2002). Structure of the epidermal growth factor receptor kinase domain alone and in complex with a 4-anilinoquinazoline inhibitor. Journal of Biological Chemistry, 277(48), 46265–46272. https://doi.org/10.1074/jbc.M207135200

Topalan, E., Büyükgüngör, A., Çiğdem, M., Güra, S., Sever, B., Otsuka, M., Fujita, M., Demirci, H., & Ciftci, H. (2025). A structural insight into two important ErbB receptors (EGFR and HER2) and their relevance to non-small cell lung cancer. Archiv der Pharmazie. Advance online publication. https://doi.org/10.1002/ardp.202400992

Van der Geer, P., Hunter, T., & Lindberg, R. A. (1994). Receptor protein-tyrosine kinases and their signal transduction pathways. Annual Review of Cell Biology, 10(1), 251–337. https://doi.org/10.1146/annurev.cb.10.110194.001343

Wang, K., Fu, Z., Sun, G., et al. (2024). Systemic treatment options for non-small cell lung cancer after failure of previous immune checkpoint inhibitors: A Bayesian network meta-analysis based on randomized controlled trials. BMC Immunology, 25(1), 37. https://doi.org/10.1186/s12865-024-00633-z

Weber, P. C. (1991). Principles of protein crystallization. Advances in Protein Chemistry, 41, 1–36. https://doi.org/10.1016/S0065-3233(08)60157-3

Westover, D., Zugazagoitia, J., Cho, B. C., Lovly, C. M., & Paz-Ares, L. (2018). Mechanisms of acquired resistance to first- and second-generation EGFR tyrosine kinase inhibitors. Annals of Oncology, 29(suppl_1), i10–i19. https://doi.org/10.1093/annonc/mdx703

Wilson, K. J., Gilmore, J. L., Foley, J., Lemmon, M. A., & Riese, D. J. (2009). Functional selectivity of EGF family peptide growth factors: Implications for cancer. Pharmacology & Therapeutics, 122(1), 1–8. https://doi.org/10.1016/j.pharmthera.2008.11.008

Yarden, Y., & Pines, G. (2012). The ERBB network: At last, cancer therapy meets systems biology. Nature Reviews Cancer, 12(8), 553–563. https://doi.org/10.1038/nrc3309

Yarden, Y., & Sliwkowski, M. X. (2001). Untangling the ErbB signalling network. Nature Reviews Molecular Cell Biology, 2(2), 127–137. https://doi.org/10.1038/35052073

Yu, H. A., Arcila, M. E., Rekhtman, N., Sima, C. S., Zakowski, M. F., Pao, W., Kris, M. G., Miller, V. A., Ladanyi, M., & Riely, G. J. (2013). Analysis of tumor specimens at the time of acquired resistance to EGFR-TKI therapy in 155 patients with EGFR-mutant lung cancers. Clinical Cancer Research, 19(8), 2240–2247. https://doi.org/10.1158/1078-0432.CCR-12-2246

Yu, Y., Yang, Y., Li, H., & Fan, Y. (2023). Targeting HER2 alterations in non-small cell lung cancer: Therapeutic breakthrough and challenges. Cancer Treatment Reviews, 114, 102520. https://doi.org/10.1016/j.ctrv.2023.102520

Yun, C. H., Mengwasser, K. E., Toms, A. V., Woo, M. S., Greulich, H., Wong, K. K., Meyerson, M., & Eck, M. J. (2007). The T790M mutation in EGFR kinase causes drug resistance by increasing the affinity for ATP. Proceedings of the National Academy of Sciences, 105(6), 2070–2075. https://doi.org/10.1073/pnas.0709662105

Appendix A: **CHEMICALS**

Table A1. 1:

Ampicillin	GOLDBIO
Chloramphenicol	GOLDBIO
Kanamycin	GOLDBIO
Glycerol	ISOLAB
Imidazole	BioFroxx
IPTG	GOLDBIO
LB Agar	Caisson
NaCl	ISOLAB
HCl	ISOLAB
Ni-NTA	QIAGEN
Paraffin Oil	Tekkim Kimya
Sarkosyl	Sigma-Aldrich
SDS	Sigma-Aldrich
Tris Base	Sigma-Aldrich
Triton X-100	Sigma-Aldrich
Tryptone	BD Biosciences
Urea	ISOLAB
Yeast Extract	BD Biosciences

Appendix B: **EQUIPMENTS**

Table B1. 1:

AKTA Go Junior	Cytiva
AKTA	Cytiva
Beckman Allegra 15R Centrifuge	Beckman Coulter
Beckman Avanti J-26S	Beckman Coulter
Beckman OptimaTM L-80 XP Ultracentrifuge	Beckman Coulter
Beckman Ti-45 Rotor	Beckman Coulter
Branson W250 Sonifier	Branson
Cryotubes	Wuxi NEST Biotechnology
Eppendorf Tubes	Eppendorf New Brunswick
Falcon Tubes	FIRATMED
Innova 44R Incubator Shaker	Eppendorf New Brunswick
Innova 4430R Incubator Shaker	Eppendorf New Brunswick
Kimtech Science KimWipes	Kimberly-Clark
NanoDropTM 2000c	Thermo Scientific
Terasaki Plates	Greiner Bio-One
TGX-Mini Protean Gradient SDS-PAGE System	Bio-Rad Laboratories
Rigaku XtaLAB Synergy Flow XRD	Rigaku
SuperdexTM200 Increase Column	Cytiva

Appendix C: **PROTEIN LADDER**

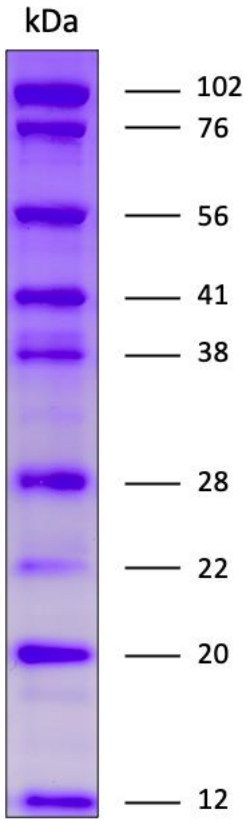

Figure C1. 1: KUYBIIG-M Protein Ladder. 15% SDS gel (2 µL/well)

Appendix D: **CRYSTALLIZATION SCREENING CONDITIONS**

Table D1. 1

3D Structure Screen	Molecular Dimensions
Additive Screen	Hampton Research
Clear Strategy Screen	Molecular Dimensions
CryoPro	Hampton Research
Crystal Screen	Hampton Research
Crystal Screen Cryo	Hampton Research
Detergent Screen	Hampton Research
Grid Screen Ammonium Sulfate	Hampton Research
Grid Screen MPD	Hampton Research
Grid Screen PEG/LiCl	Hampton Research
Grid Screen PEG6000	Hampton Research
Grid Screen Sodium Chloride	Hampton Research
Helix	Molecular Dimensions
Index	Hampton Research
Ionic Liquid Screen	Hampton Research
JBScreen Nuc-Pro	Jena Bioscience
JCSG	Molecular Dimensions
MacroSol	Molecular Dimensions
MembFac	Hampton Research
MIDAS	Molecular Dimensions
Morpheus	Molecular Dimensions
MultiXtal	Molecular Dimensions
Natrix	Hampton Research
NeXtal Protein Complex Suite	NeXtal Biotechnologies

NR-LBD	Molecular Dimensions
PACT Premier	Molecular Dimensions
PEG/Ion	Hampton Research
PEGRx	Hampton Research
PGA Screen	Molecular Dimensions
ProPlex Screen	Molecular Dimensions
Quick Screen	Hampton Research
SaltRx	Hampton Research
Structure Screen	Molecular Dimensions
Stura FootPrint Screen	Molecular Dimensions
Wizard	Rigaku
Wizard Cryo	Rigaku
Wizard Precipitant Synergy	Rigaku